$B \rightarrow D\ell\nu$ form factors at nonzero recoil and $|V_{cb}|$ from 2 + 1-flavor lattice QCD

Jon A. Bailey,[1] A. Bazavov,[2,*] C. Bernard,[3] C. M. Bouchard,[4,5] C. DeTar,[6,†] Daping Du,[7,8] A. X. El-Khadra,[7]
J. Foley,[6] E. D. Freeland,[9] E. Gámiz,[10] Steven Gottlieb,[11] U. M. Heller,[12] J. Komijani,[3] A. S. Kronfeld,[13,14]
J. Laiho,[8] L. Levkova,[6] P. B. Mackenzie,[13] E. T. Neil,[15,16] Si-Wei Qiu,[6,‡] J. Simone,[13] R. Sugar,[17] D. Toussaint,[18]
R. S. Van de Water,[13] and Ran Zhou[11,13]

(Fermilab Lattice and MILC Collaborations)

[1]Department of Physics and Astronomy, Seoul National University, Seoul 151-742, South Korea
[2]Physics Department, Brookhaven National Laboratory, Upton, New York 11973, USA
[3]Department of Physics, Washington University, St. Louis, Missouri 63130, USA
[4]Physics Department, College of William and Mary, Williamsburg, Virginia 23187, USA
[5]Department of Physics, The Ohio State University, Columbus, Ohio 43210, USA
[6]Department of Physics and Astronomy, University of Utah, Salt Lake City, Utah 84112, USA
[7]Department of Physics, University of Illinois, Urbana, Illinois 61801, USA
[8]Department of Physics, Syracuse University, Syracuse, New York 13244, USA
[9]Liberal Arts Department, School of the Art Institute of Chicago, Chicago, Illinois 60603, USA
[10]CAFPE and Departamento de Física Teórica y del Cosmos, Universidad de Granada,
Granada E-18002, Spain
[11]Department of Physics, Indiana University, Bloomington, Indiana 47405, USA
[12]American Physical Society, Ridge, New York 11961, USA
[13]Fermi National Accelerator Laboratory, Batavia, Illinois 60510, USA
[14]Institute for Advanced Study, Technische Universität München, 85748 Garching, Germany
[15]Department of Physics, University of Colorado, Boulder, Colorado 80309, USA
[16]RIKEN-BNL Research Center, Brookhaven National Laboratory, Upton, New York 11973, USA
[17]Department of Physics, University of California, Santa Barbara, California 93106, USA
[18]Department of Physics, University of Arizona, Tucson, Arizona 85721, USA

We present the first unquenched lattice-QCD calculation of the hadronic form factors for the exclusive decay $\bar{B} \rightarrow D\ell\bar{\nu}$ at nonzero recoil. We carry out numerical simulations on 14 ensembles of gauge-field configurations generated with $2 + 1$ flavors of asqtad-improved staggered sea quarks. The ensembles encompass a wide range of lattice spacings (approximately 0.045 to 0.12 fm) and ratios of light (up and down) to strange sea-quark masses ranging from 0.05 to 0.4. For the b and c valence quarks we use improved Wilson fermions with the Fermilab interpretation, while for the light valence quarks we use asqtad-improved staggered fermions. We extrapolate our results to the physical point using rooted staggered heavy-light meson chiral perturbation theory. We then parametrize the form factors and extend them to the full kinematic range using model-independent functions based on analyticity and unitarity. We present our final results for $f_+(q^2)$ and $f_0(q^2)$, including statistical and systematic errors, as coefficients of a series in the variable z and the covariance matrix between these coefficients. We then fit the lattice form-factor data jointly with the experimentally measured differential decay rate from $BABAR$ to determine the CKM matrix element, $|V_{cb}| = (39.6 \pm 1.7_{\text{QCD+exp}} \pm 0.2_{\text{QED}}) \times 10^{-3}$. As a byproduct of the joint fit we obtain the form factors with improved precision at large recoil. Finally, we use them to update our calculation of the ratio $R(D)$ in the Standard Model, which yields $R(D) = 0.299(11)$.

PACS numbers: 12.38.Gc, 13.20.He, 12.15.Hh

I. INTRODUCTION

Precision tests of the Standard Model (SM) seek to find discrepancies that may indicate the presence of new physics. The SM requirement of a unitary Cabibbo–Kobayashi–Maskawa (CKM) weak mixing matrix provides a good opportunity for such a test. The unitarity-triangle test checks the orthogonality of the first and third rows of

*Present address: Department of Physics and Astronomy, University of Iowa, Iowa City, IA, USA.
†detar@physics.utah.edu
‡Present address: Laboratory of Biological Modeling, NIDDK, NIH, Bethesda, Maryland, USA.
qiu@physics.utah.edu

the CKM matrix. It requires consistency between results extracted from the experimental measurements and theoretical calculations of a wide variety of flavor- and *CP*-violating observables. Although recent results have been roughly consistent with unitarity [1,2], some disagreements persist and require further attention. The CKM parameter $|V_{cb}|$ plays an important role in the unitarity triangle test, since it normalizes the lengths of sides of the triangle and contributes to tension in the unitarity constraint.

The SM parameter $|V_{cb}|$ is determined through the combination of an experimental measurement of a branching fraction and the theoretical calculation of the underlying hadronic form factor(s). There are two common approaches [3] using (1) the exclusive processes $\bar{B} \to D\ell\nu$ and $\bar{B} \to D^*\ell\bar{\nu}$ with lattice-QCD determinations of the relevant hadronic form factors [4,5] or (2) the inclusive decay $\bar{B} \to X_c\ell\bar{\nu}$ to any charm-containing final state X_c and the operator-product and heavy-quark expansions to describe strong-interaction effects [6,7]. It is troublesome that the most recent results for $|V_{cb}|$ from these exclusive and inclusive determinations disagree at the 3σ level [3,5]. It is unlikely that this difference is due to new physics effects [8], and further work is needed to refine the determinations.

Reducing the error in the determination of $|V_{cb}|$ requires both experimental and theoretical effort. Recent work by the *BABAR* Collaboration [9] has provided better measurements of the decay rate. The latest results from the Belle Collaboration for this process are still preliminary [10]. Further improvements will come from Belle II. In this work we improve the exclusive determination of $|V_{cb}|$ from the decay process $\bar{B} \to D\ell\bar{\nu}$ by providing the first unquenched lattice-QCD calculation of the relevant form factors with a complete error budget and small statistical and systematic errors.

Traditionally, experimental measurements are first extrapolated to zero recoil, where the comparison with theory to obtain $|V_{cb}|$ occurs, using a parametrization of the momentum dependence from Caprini, Lellouch, and Neubert (CLN) [11]. Indeed lattice calculations at zero recoil momentum are simpler, and for the exclusive process $\bar{B} \to D^*\ell\bar{\nu}$ this method yields a very precise determination of $|V_{cb}|$, which is described in our companion work [5]. However, due to the more severe phase space suppression of the $\bar{B} \to D\ell\bar{\nu}$ rate near zero recoil (compared with $\bar{B} \to D^*\ell\bar{\nu}$) the extrapolation of the experimental data to zero recoil is a source of significant uncertainty. This results in determinations of $|V_{cb}|$ from $\bar{B} \to D\ell\bar{\nu}$ that are less precise than they have to be. Here we calculate the form factors for $\bar{B} \to D\ell\bar{\nu}$ for a range of recoil momenta and parametrize their dependence on momentum transfer using the model-independent *z* expansion of Boyd, Grinstein and Lebed [12]. We fit the experimental and lattice data together as a function of momentum transfer and determine

$|V_{cb}|$ from the relative normalization over the entire range of recoil momenta.

Where previous calculations of this process at nonzero recoil ignored effects of sea quarks [13], ours includes them. The use of asqtad-improved staggered fermions and improved Wilson ("clover") quarks reduces lattice discretization errors. A preliminary determination of $|V_{cb}|$ from $\bar{B} \to D\ell\bar{\nu}$ with a very small subset of the present asqtad ensembles was presented in Ref. [14]. That calculation was done only at zero recoil and used only lattices with spacing approximately 0.12 fm, so a continuum extrapolation was not possible. The broad range of lattice spacings and sea-quark-mass ratios in our current study gives confidence in the extrapolation to physical quark masses and zero lattice spacing. More recently, in a related project of ours [15], the ratio of form factors for $B_s \to D_s\ell\nu$ to $B \to D\ell\nu$ decays was obtained using only four asqtad ensembles, i.e., with two different light sea-quark masses at two lattice spacings. This data set was also used to obtain the first Standard-Model prediction for $R(D) \equiv \mathcal{B}(B \to D\tau\nu)/\mathcal{B}(B \to D\ell\nu)$ from unquenched lattice QCD in Ref. [16]. The present work uses all 14 ensembles and uses a slightly different analysis. These are the first such calculations to combine all of the ingredients listed above.

Preliminary results for the $B \to D$ form factors from this project were presented in [4]. The final analysis presented here includes a more sophisticated treatment of the matching factors as well as more refined estimates for the renormalization and heavy-quark discretization errors.

This article is organized as follows. In Sec. II we review the formalism and our strategy for extracting the form factors at nonzero recoil. In Sec. III we give details of the ensembles and simulation and discuss our determination of the form factors and the chiral-continuum extrapolation. We discuss systematic errors in Sec. IV. In Sec. V we present fits to our lattice data for the two form factors f_+ and f_0 and a joint fit that combines our lattice data with the 2009 *BABAR* measurements [9], leading, finally, to our result for $|V_{cb}|$. We discuss our results in Sec. VI. Appendix A discusses technical details regarding the tuning of the bare-quark masses. Appendix B derives the pattern of heavy-quark discretization effects and discusses some details of matching lattice gauge theory with heavy quarks to continuum QCD.

II. FORM FACTORS

A. Continuum form factors

The hadronic interaction in the process $\bar{B} \to D\ell\bar{\nu}$ is determined by the transition matrix element of the vector current $\mathcal{V}^\mu = \bar{c}\gamma^\mu b$, which is conventionally decomposed in terms of the vector and scalar form factors $f_+(q^2)$ and $f_0(q^2)$ as

$$\langle D(p_D)|\mathcal{V}^\mu|B(p_B)\rangle$$
$$= f_+(q^2)\left[(p_B + p_D)^\mu - \frac{M_B^2 - M_D^2}{q^2}q^\mu\right]$$
$$+ f_0(q^2)\frac{M_B^2 - M_D^2}{q^2}q^\mu. \tag{2.1}$$

Here p_B and p_D are the momenta of the B and D mesons, M_B and M_D are the respective masses, and $q = p_B - p_D$ is the momentum transferred to the leptons. In the approximation that the masses of the leptons $\ell = e, \mu, \nu_e, \nu_\mu$ are much smaller than the B and D mass difference $M_B - M_D$, the differential decay rate is

$$\frac{d\Gamma}{dw}(\bar{B} \to D\ell\bar{\nu})$$
$$= |\bar{\eta}_{EW}|^2 \frac{G_F^2|V_{cb}|^2 M_B^5}{48\pi^3}(w^2 - 1)^{3/2} r^3 (1+r)^2 \mathcal{G}(w)^2, \tag{2.2}$$

where $|\bar{\eta}_{EW}|^2$ accounts for electroweak corrections discussed below, G_F is the Fermi weak decay constant, $|V_{cb}|$ is the desired CKM matrix element, $w = v \cdot v'$ is the recoil parameter, $v = p_B/M_B$ and $v' = p_D/M_D$ are the hadronic velocities, and $\mathcal{G}$ is related to f_+ through

$$f_+(w)^2 = \frac{(1+r)^2}{4r}\mathcal{G}(w)^2 \tag{2.3}$$

with $r \equiv M_D/M_B = 0.354$.

The alternative parametrization in terms of the form factors h_+ and h_- is convenient in heavy-quark effective theory (HQET) and heavy-light meson chiral perturbation theory:

$$\frac{\langle D(p_D)|\mathcal{V}^\mu|B(p_B)\rangle}{\sqrt{M_B M_D}} = h_+(w)(v + v')^\mu + h_-(w)(v - v')^\mu. \tag{2.4}$$

These form factors are related to f_+ and f_0 through

$$f_+(q^2) = \frac{1}{2\sqrt{r}}[(1+r)h_+(w) - (1-r)h_-(w)], \tag{2.5}$$

$$f_0(q^2) = \sqrt{r}\left[\frac{w+1}{1+r}h_+(w) - \frac{w-1}{1-r}h_-(w)\right], \tag{2.6}$$

where $q^2 = M_B^2 + M_D^2 - 2wM_BM_D$. We note, also, the kinematic constraint $f_+(0) = f_0(0)$ at $q^2 = 0$, which corresponds to $w = (M_B^2 + M_D^2)/(2M_BM_D) \approx 1.59$. We also have

$$\mathcal{G}(w) = h_+(w) - \left(\frac{1-r}{1+r}\right)h_-(w). \tag{2.7}$$

B. Form factors from lattice matrix elements

We use the local Fermilab-improved vector current for the quark transition $x \to y$

$$V_{xy}^\mu = \bar{\Psi}_x \gamma^\mu \Psi_y, \tag{2.8}$$

where the subscripts denote flavor, Ψ is the "rotated" field [17]

$$\Psi = (1 + d_1 \boldsymbol{\gamma} \cdot \boldsymbol{D}_{\text{lat}})\psi, \tag{2.9}$$

and ψ is the heavy-quark field in the action. The lattice current V^μ is related to the continuum current $\mathcal{V}^\mu$ through

$$Z_{xy}^\mu V_{xy}^\mu \doteq \mathcal{V}_{xy}^\mu, \tag{2.10}$$

where "$\doteq$" denotes the equality of matrix elements. Following Refs. [18] and [19], we define the correction matching factor as the double ratio of matching factors for flavor off-diagonal currents to those for flavor-diagonal currents:

$$\rho_{V^\mu}^2 = \frac{Z_{V_{cb}^\mu}Z_{V_{bc}^\mu}}{Z_{V_{cc}^4}Z_{V_{bb}^4}}, \tag{2.11}$$

where $\rho_{V^\mu} = 1 + 4\pi\alpha_s(q^*)\rho_{V^\mu}^{[1]} + \mathcal{O}(\alpha_s(q^*)^2)$ is determined to one-loop order in lattice perturbation theory [19]. It is found to be quite close to 1 because of cancellations in the ratio of similar quantities, including cancellations of tadpole diagrams. The truncation error is expected to be small because $\alpha_s(q^* = 2/a) \approx 0.2$.

The matching factor $\rho_{V^\mu}(w)$ depends, in principle, upon the velocity transfer w. At present we have calculated only $\rho_{V^4}(1)$ for the quark masses and lattice spacings in our project. Calculation of the spatial correction ρ_{V^i} is more difficult because, even for zero recoil, one must calculate it for nonzero momentum. Thus we have calculated $\rho_{V^i}(1)$ only for the simpler case $m_c a = 0$, but our lack of knowledge of the m_c dependence of the one-loop correction to ρ_{V^i} makes only a small contribution to our final uncertainty. The w dependence of ρ_{V^i} is also unavailable. Below we note where these issues arise.

To compute the form factors h_+ and h_- at arbitrary recoil, we need the lattice matrix elements of both the temporal and spatial vector currents, V^4 and V. In practice, we use ratios of lattice correlators in which the flavor-conserving renormalization factors are automatically included, as discussed below. These ratios also suppress statistical fluctuations and systematic errors. The remaining correction factors ρ_{V^4} and ρ_{V^i} are applied after fitting the ratios. We apply this correction in Sec. III F.

Our calculation is done in the B-meson rest frame for any D-meson recoil momentum $\boldsymbol{p}$. We compute the double ratio

$$R_+ = \frac{\langle D(\boldsymbol{0})|V_{cb}^4|B(\boldsymbol{0})\rangle\langle B(\boldsymbol{0})|V_{cb}^4|D(\boldsymbol{0})\rangle}{\langle D(\boldsymbol{0})|V_{cc}^4|D(\boldsymbol{0})\rangle\langle B(\boldsymbol{0})|V_{bb}^4|B(\boldsymbol{0})\rangle} \qquad (2.12)$$

and the single ratios

$$Q_+(\boldsymbol{p}) \equiv \frac{\langle D(\boldsymbol{p})|V^4|B(\boldsymbol{0})\rangle}{\langle D(\boldsymbol{0})|V^4|B(\boldsymbol{0})\rangle}, \qquad (2.13)$$

$$R_-(\boldsymbol{p}) \equiv \frac{\langle D(\boldsymbol{p})|V|B(\boldsymbol{0})\rangle}{\langle D(\boldsymbol{p})|V^4|B(\boldsymbol{0})\rangle}, \qquad (2.14)$$

$$x_f(\boldsymbol{p}) \equiv \frac{\langle D(\boldsymbol{p})|V|D(\boldsymbol{0})\rangle}{\langle D(\boldsymbol{p})|V^4|D(\boldsymbol{0})\rangle}. \qquad (2.15)$$

Note that $Q_+(\boldsymbol{p})$ is the ratio of $B \to D$ matrix elements at nonzero and zero recoil, and that $x_f(\boldsymbol{p})$ is computed only from the flavor-diagonal transition $D \to D$. As spelled out below, we use $R_+(\boldsymbol{p})$, $Q_+(\boldsymbol{p})$, and $R_-(\boldsymbol{p})$ to obtain $h_+(w)$ and $h_-(w)$, and $x_f(\boldsymbol{p})$ to obtain the recoil w. The flavor-conserving renormalization factors $Z_{V_{bb}^4}$ and $Z_{V_{cc}^4}$ cancel exactly in the double ratio R_+, which was introduced by Hashimoto *et al.* and used to obtain the $B \to D\ell\nu$ form factor at zero recoil in quenched lattice QCD [20].

From Eq. (B15), the 3-vector $\boldsymbol{x}_f$ yields the velocity without any matching ambiguities:

$$\boldsymbol{x}_f = \frac{\boldsymbol{v}'}{w+1}. \qquad (2.16)$$

Because $w^2 = 1 + \boldsymbol{v}'^2$ (when the initial meson is at rest), one finds

$$w(\boldsymbol{p}) = \frac{1 + x_f^2(\boldsymbol{p})}{1 - x_f^2(\boldsymbol{p})}. \qquad (2.17)$$

Thus, even the kinematic variable w is determined dynamically from a ratio of matrix elements.

The other ratios require matching factors. It is convenient to define

$$\mathcal{R}_+ = \rho_{V^4}^2(1)R_+, \qquad (2.18)$$

$$\mathcal{Q}_+(\boldsymbol{p}) = \frac{\rho_{V^4}(w)}{\rho_{V^4}(1)}Q_+(\boldsymbol{p}), \qquad (2.19)$$

$$\mathcal{R}_-(\boldsymbol{p}) = \frac{\rho_{V^i}(w)}{\rho_{V^4}(w)}R_-(\boldsymbol{p}). \qquad (2.20)$$

We derive these factors and discuss how we handle them in Appendix B. Note that $\mathcal{R}_+$ reduces to

$$\sqrt{\mathcal{R}_+} = h_+(1) + \text{matching and discretization errors.} \qquad (2.21)$$

Also, $\mathcal{Q}_+(\boldsymbol{0}) = Q_+(\boldsymbol{0}) = 1$ by construction. We then can obtain h_+ and h_- from

$$h_+(w(\boldsymbol{p})) = \sqrt{\mathcal{R}_+}\mathcal{Q}_+(\boldsymbol{p})[1 - \mathcal{R}_-(\boldsymbol{p}) \cdot \boldsymbol{x}_f(\boldsymbol{p})], \qquad (2.22)$$

$$h_-(w(\boldsymbol{p})) = \sqrt{\mathcal{R}_+}\mathcal{Q}_+(\boldsymbol{p})\left[1 - \frac{\mathcal{R}_-(\boldsymbol{p}) \cdot \boldsymbol{x}_f(\boldsymbol{p})}{x_f^2(\boldsymbol{p})}\right], \qquad (2.23)$$

as in Eq. (2.21) up to matching and discretization errors.

III. ANALYSIS

A. Lattice action and parameters

Our calculation uses 14 ensembles of gauge-field configurations generated in the presence of $2 + 1$ flavors of asqtad-improved staggered sea quarks by the MILC Collaboration [21–23]. Ensembles are indicated graphically in Fig. 1, and they are tabulated in Table I. There are four lattice spacings, $a \approx 0.12$ fm, 0.09 fm, 0.06 fm, and 0.045 fm, and light sea-quark to strange sea-quark mass ratios $\hat{m}'/m_s'$ ranging from 0.4 to 0.05. The strange sea-quark mass is set approximately to its physical value. For the light valence quarks we use the asqtad action. Light-quark propagators are converted to improved "naive" propagators as in Ref. [24] to implement the standard Dirac spin algebra. In this study, masses of the light valence quarks are always equal to the sea-quark masses. For the heavy valence quarks we use the Fermilab interpretation of the clover action with the parameters listed in Table II.
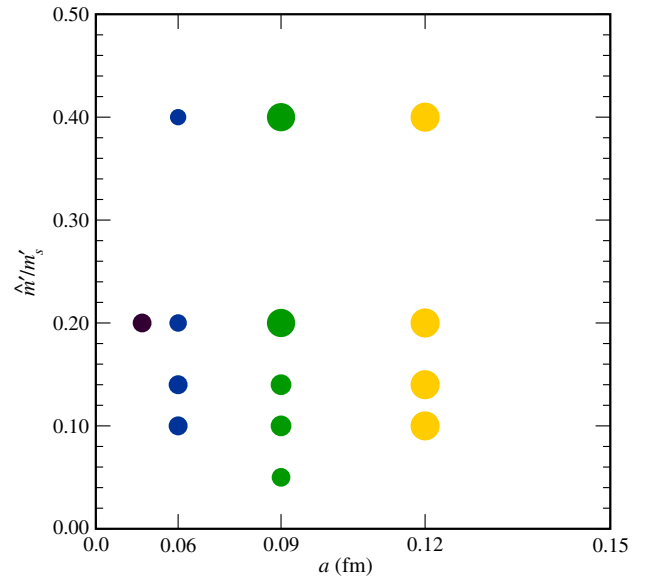

FIG. 1 (color online). Range of lattice spacings and light-quark masses used here. The area of each disk is proportional to the number of configurations in the ensemble.

TABLE I. Parameters of the lattice-gauge-field ensembles. The columns from left to right are the approximate lattice spacing in fm, the bare sea-quark masses in lattice units $a\hat{m}'/am'_s$, the lightest pseudoscalar in MeV, the root-mean-square (rms) mass of the pion taste multiplet in MeV, the dimensionless factor $M_\pi^P L$, the dimensions of the lattice in lattice units, the number of configurations in each ensemble (four sources each), and the tadpole-improvement factor u_0 (obtained from the average plaquette).

a (fm)	$a\hat{m}'/am'_s$	M_π^P (MeV)	M_π^{RMS} (MeV)	$M_\pi^P L$	Lattice size	Configs	u_0	data DOI
≈ 0.12	0.02/0.05	560	670	6.2	$20^3 \times 64$	2052	0.8688	[25]
	0.01/0.05	390	540	4.5	$20^3 \times 64$	2259	0.8677	[26]
	0.007/0.05	320	500	3.8	$20^3 \times 64$	2110	0.8678	[27]
	0.005/0.05	270	470	3.8	$24^3 \times 64$	2099	0.8678	[28]
≈ 0.09	0.0124/0.031	500	550	5.8	$28^3 \times 96$	1996	0.8788	[29]
	0.0062/0.031	350	420	4.1	$28^3 \times 96$	1931	0.8782	[30]
	0.00465/0.031	310	380	4.1	$32^3 \times 96$	984	0.8781	[31]
	0.0031/0.031	250	330	4.2	$40^3 \times 96$	1015	0.8779	[32]
	0.00155/0.031	180	280	4.8	$64^3 \times 96$	791	0.877805	[33]
≈ 0.06	0.0072/0.018	450	470	6.3	$48^3 \times 144$	593	0.8881	[34]
	0.0036/0.018	320	340	4.5	$48^3 \times 144$	673	0.88788	[35]
	0.0025/0.018	260	290	4.4	$56^3 \times 144$	801	0.88776	[36]
	0.0018/0.018	220	260	4.3	$64^3 \times 144$	827	0.88764	[37]
≈ 0.045	0.0028/0.014	320	330	4.6	$64^3 \times 192$	801	0.89511	[38]

TABLE II. Parameters of the heavy valence quarks. The approximate lattice spacing and bare sea-quark masses in the first two columns identify the ensemble. The remaining columns show the coefficient of the clover term in the SW action c_{SW}, the bare hopping-parameter κ, and the rotation parameter in the current d_1. The primes on κ distinguish the simulation from the physical values.

$\approx a$ (fm)	$a\hat{m}'/am'_s$	c_{SW}	κ'_b	d_{1b}	κ'_c	d_{1c}
0.12	0.02/0.05	1.525	0.0918	0.09439	0.1259	0.07539
0.12	0.01/0.05	1.531	0.0901	0.09334	0.1254	0.07724
0.12	0.007/0.05	1.530	0.0901	0.09332	0.1254	0.07731
0.12	0.005/0.05	1.530	0.0901	0.09332	0.1254	0.07733
0.09	0.0124/0.031	1.473	0.0982	0.09681	0.1277	0.06420
0.09	0.0062/0.031	1.476	0.0979	0.09677	0.1276	0.06482
0.09	0.00465/0.031	1.477	0.0977	0.09671	0.1275	0.06523
0.09	0.0031/0.031	1.478	0.0976	0.09669	0.1275	0.06537
0.09	0.00155/0.031	1.4784	0.0976	0.09669	0.1275	0.06543
0.06	0.0072/0.018	1.4276	0.1048	0.09636	0.1295	0.05078
0.06	0.0036/0.018	1.4287	0.1052	0.09631	0.1296	0.05055
0.06	0.0025/0.018	1.4293	0.1052	0.09633	0.1296	0.05070
0.06	0.0018/0.018	1.4298	0.1052	0.09635	0.1296	0.05076
0.045	0.0028/0.014	1.3943	0.1143	0.08864	0.1310	0.03842

Two-point and three-point correlators are computed from four equally spaced source times per configuration, but with random offsets in time and space to reduce correlations between successive gauge-field configurations within an ensemble. We performed a blocking study to look for residual autocorrelations, and found that the statistical errors did not change significantly with block size. Thus we do not block the data in this work. The masses of the heavy valence quarks were tuned so that the kinetic masses of the D_s and B_s mesons were equal to their physical values. A detailed discussion of tuning is given in the appendix of Ref. [5], where we show that we get good

agreement between the lattice values of the D_s and B_s hyperfine splittings and their experimental values. The simulation values of the heavy-quark masses are not quite the same as our best-tuned values, which were determined *a posteriori*. Postsimulation adjustment for heavy-quark-mass tuning is described in Sec. III D.

After fixing the lattices to Coulomb gauge, two types of interpolating operators for the D meson are used, namely, a local operator and a smeared operator based on a Richardson 1S wave function [39]. For the B meson we use only the 1S operator. These two operators have different overlap with excited states, so computing both

helps us remove excited-state contributions. We generate three-point functions in a standard way by fixing the position of the D and B mesons to a separation T in imaginary time and then varying the time t of the vector current. Calculations at two adjacent time separations T are carried out in each case to control the effects of oscillating staggered-fermion propagators. We rotate the heavy-quark fields as in Eq. (2.9) using the tadpole-improved tree-level values for d_1 listed in Table II, so that the vector current is tree-level improved. Calculations are made at several choices of three-momentum. In units of $2\pi/L$, for this study we use five momenta (0,0,0), (0,0,1), (0,1,1), (1,1,1), and (2,0,0). Results at larger momenta tend to have significantly larger statistical errors, and also suffer from larger momentum-dependent discretization errors. In the two-point correlator these momenta are projected at the sink and in the three-point correlator, at the current. In the latter case the three-momentum of the B meson is set to zero.

B. Fitting strategy

We need both two-point and three-point correlation functions to construct the form factor introduced in Sec. II B. We use interpolating operators $\mathcal{O}_{Xa}(\boldsymbol{p}, t)$ of spatial momentum $\boldsymbol{p}$ and time t with $X \in \{B, D\}$ and $a \in \{1S, d\}$. The notation d signifies a delta function (point) source, while $1S$ denotes a 1S Richardson wavefunction. See Ref. [40] for details. The correlation functions can be expressed in terms of operator matrix elements:

$$C^{2\text{pt},Xa \to Xb}(\boldsymbol{p}, t) = \langle \mathcal{O}_{Xb}^{\dagger}(\boldsymbol{p}, 0) \mathcal{O}_{Xa}(\boldsymbol{p}, t) \rangle, \quad (3.1)$$

$$C_{\mu}^{3\text{pt},Xa \to Yb}(\boldsymbol{p}, t) = \langle \mathcal{O}_{Yb}^{\dagger}(-\boldsymbol{p}, 0) V^{\mu}(\boldsymbol{p}, t) \mathcal{O}_{Xa}(\boldsymbol{0}, T) \rangle, \quad (3.2)$$

where T is the imaginary time separation between the B and D mesons.

The spectral decomposition of the two-point correlator is

$$C^{2\text{pt},Xa \to Xb}(\boldsymbol{p}, t) = \sum_{n} s_n(t) \frac{\sqrt{Z_{Xa,n}(\boldsymbol{p}) Z_{Xb,n}(\boldsymbol{p})}}{2 E_n(\boldsymbol{p})}$$
$$\times [\exp(-E_n(\boldsymbol{p}) t) + \exp(-E_n(\boldsymbol{p})(N_t - t))], \quad (3.3)$$

where there are either nonoscillating terms with $s_n(t) = 1$ or staggered-fermion opposite-parity oscillating terms $s_n(t) = -(-1)^t$, N_t is the lattice extent in time, and $Z_{Xa,n}$ is the overlap coefficient. For the three-point function, the decomposition is similar:

$$C_{\mu}^{3\text{pt},Xa \to Yb}(\boldsymbol{p}, t) = \sum_{n,m} s_n(t) s_m(T - t) \sqrt{Z_{Yb,n}(\boldsymbol{p})}$$
$$\times \frac{e^{-E_n(p)t}}{\sqrt{2 E_n(\boldsymbol{p})}} \langle Yb, n(\boldsymbol{p}) | V^{\mu} | Xa, m(\boldsymbol{0}) \rangle$$
$$\times \frac{e^{-M_m(T-t)}}{\sqrt{2 M_m}} \sqrt{Z_{Xa,m}(\boldsymbol{0})}, \quad (3.4)$$

where we have assumed $t < T \ll N_t$, so we may neglect wraparound terms with $t \to N_t - t$ and $T - t \to N_t - (T - t)$.

The double ratio R_+ can be calculated very precisely from

$$R_{+,b}(t, T) = \frac{C_4^{3\text{pt},B,1S \to Db}(\boldsymbol{0}, t) C_4^{3\text{pt},Db \to B,1S}(\boldsymbol{0}, t)}{C_4^{3\text{pt},Db \to Db}(\boldsymbol{0}, t) C_4^{3\text{pt},B,1S \to B,1S}(\boldsymbol{0}, t)}. \quad (3.5)$$

This quantity depends on t, T and the D-meson interpolating operator, labeled by b. The dependence arises from contributions from excited states and opposite-parity oscillating states. As in Refs. [5,41] and [42] we suppress contributions from oscillating states by averaging

$$\bar{R}_{+,b}(t, T) \equiv \frac{1}{2} R_{+,b}(t, T) + \frac{1}{4} R_{+,b}(t, T + 1)$$
$$+ \frac{1}{4} R_{+,b}(t + 1, T + 1). \quad (3.6)$$

We drop the bar henceforth. We use a similar method for the other three-point correlation functions. We find that the suppression of oscillating states for $B \to D$ correlators is similar to that of our previous work on $B \to D^* \ell \nu$ [5]. In particular, the contribution from the first oscillating B- and D-meson excited states, which does not itself oscillate in time, is reduced by a factor of $\sim$5–12 using the average in Eq. (3.6), where greater suppression occurs for finer lattice spacings.

For large t and $T - t$, excited-state contributions are negligible, giving the desired result,

$$R_{+,b}(t, T) \to R_+, \quad (3.7)$$

as a plateau in the ratio vs t, as illustrated in Fig. 2. The leading corrections to the plateau arise from contributions from the first excited D- and B-meson states. For large t and $T - t$, their contributions to the correlator double ratio fall off as $\exp[-\Delta M t]$ and $\exp[-\Delta M(T - t)]$, where $\Delta M = \Delta M_B$ or ΔM_D, the splitting between the ground state and first excited state of the B and D mesons, respectively. Since they are both small, for fitting the ratio, we use the approximation
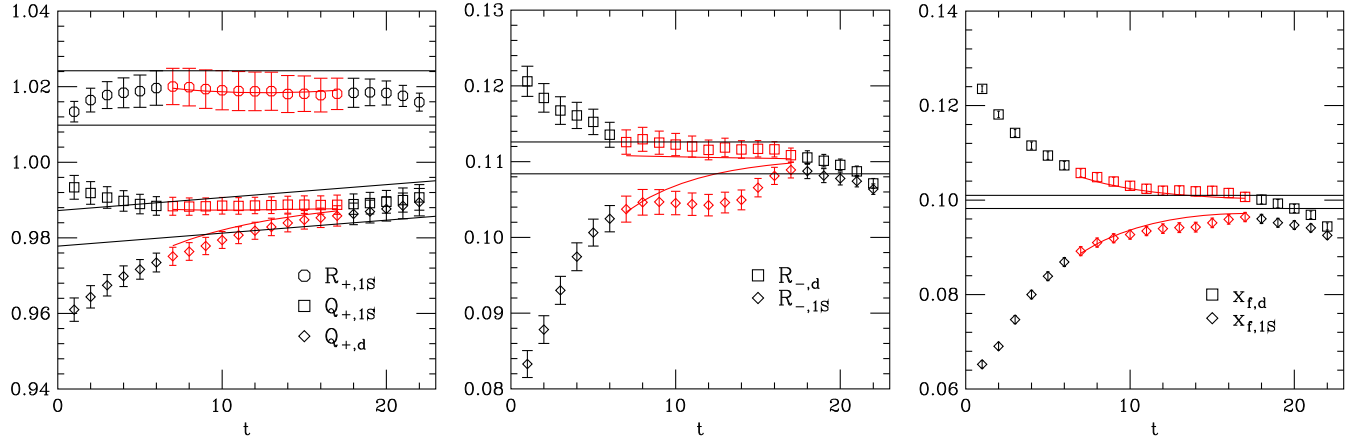
FIG. 2 (color online).   Sample joint three-point function fits for determining the ratios R_+ and $Q_+(\boldsymbol{p})$ (left), $R_-^1(\boldsymbol{p})$ (middle), and $x_f^1(\boldsymbol{p})$ (right), for lattice momentum $\boldsymbol{p} = (1,0,0)$. Data shown are for the $a \approx 0.06$ fm, $\hat{m}' = 0.14 m_s'$ ensemble with B-D separation $T = 24$ and 25. Values are plotted against the time t of the vector-current insertion. Data points at the left and right extremities are not included in the fit. A color (gray-scale) change indicates which points are included in the fit. Black lines indicate the upper and lower 1σ range of the ground-state contribution. Best fit lines are shown in red (gray). For $Q_+(\boldsymbol{p})$ the "plateau" is slanted because of the factor $\exp(\delta mt)$ in Eq. (3.10).

$$R_{+,b}(t,T) \approx R_+ + A_{R_{+,b}} \exp(-\Delta M_D t)$$
$$+ B_{R_{+,b}} \exp[-\Delta M_B(T-t)]$$
$$+ C_{R_{+,b}} \exp(-\Delta M_B t)$$
$$+ D_{R_{+,b}} \exp[-\Delta M_D(T-t)] \exp(\Delta M_B t).$$
$$(3.8)$$

However, since $\Delta M_D \approx \Delta M_B$ we construct the fit model from only the R_+, A, and B terms. We choose separations T large enough that we can safely neglect the last term.

Similarly, we introduce a time- and interpolating-operator-dependent ratio

$$Q_{+,b}(\boldsymbol{p},t,T) \equiv \frac{C_4^{\mathrm{3pt},B,1S \to Db}(\boldsymbol{p},t)}{C_4^{\mathrm{3pt},B,1S \to Db}(\boldsymbol{0},t)} \frac{E_D Z_{Db}(\boldsymbol{0})}{M_D Z_{Db}(\boldsymbol{p})} e^{(E_D - M_D)t}.$$
$$(3.9)$$

In this ratio the plateau takes on the value $Q_+(\boldsymbol{p})$ introduced in Eq. (2.13). Again, the leading corrections to the plateau arise from contributions from the first excited D- and B-meson states. For large t and $T - t$, their contributions to the correlator ratio fall off as $\exp[-\Delta E_D t]$ and $\exp[-\Delta M_B(T - t)]$. Where they are both small, for fitting the ratio, we use the approximation

$$Q_{+,b}(\boldsymbol{p},t,T) \approx Q_+(\boldsymbol{p}) \exp(\delta mt) + A_{Q_{+,b}}(\boldsymbol{p}) \exp(-\Delta E_D t)$$
$$+ B_{Q_{+,b}}(\boldsymbol{p}) \exp[-\Delta M_D t]$$
$$+ C_{Q_{+,b}}(\boldsymbol{p}) \exp[-\Delta M_B(T-t)]. \quad (3.10)$$

The parameter δm vanishes when the exponential factor in Eq. (3.9) cancels the time dependence in the three-point

functions, as it should. Since there may be slight differences in the determination of the masses from the three-point and two-point functions, the cancellation might not be perfect. Therefore, we introduce δm as a constrained fitting parameter. The prior constraint is centered at zero and it has a width determined from the small statistical error in the two-point-fitted energies. In practice, the values of $a\delta m$, are typically of order 10^{-4}.

For $\boldsymbol{R}_{-,b}(\boldsymbol{p},t,T)$ we form the ratio

$$R_{-,b}^i(\boldsymbol{p},t,T) = \frac{C_i^{\mathrm{3pt},B,1S \to Db}(\boldsymbol{p},t)}{C_4^{\mathrm{3pt},B,1S \to Db}(\boldsymbol{p},t)},$$
$$(3.11)$$

so that for large t and $T - t$ we have $\boldsymbol{R}_{-,b}(\boldsymbol{p},t,T) \to \boldsymbol{R}_-(\boldsymbol{p})$, i.e., the quantity defined in Eq. (2.14). Similarly, for $\boldsymbol{x}_f(\boldsymbol{p},t,T)$, we use the ratio

$$x_{f,b}^i(\boldsymbol{p},t,T) = \frac{C_i^{\mathrm{3pt},Db \to Db}(\boldsymbol{p},t)}{C_4^{\mathrm{3pt},Db \to Db}(\boldsymbol{p},t)},$$
$$(3.12)$$

so that $\boldsymbol{x}_{f,b}(\boldsymbol{p},t,T) \to \boldsymbol{x}_f(\boldsymbol{p})$, i.e., the quantity defined in Eq. (2.15). To fit the time dependence of $\boldsymbol{R}_{-,b}(\boldsymbol{p},t,T)$ we use

$$\boldsymbol{R}_{-,b}(\boldsymbol{p},t,T) \approx \boldsymbol{R}_-(\boldsymbol{p}) + A_{R_{-,b}}(\boldsymbol{p}) \exp(-\Delta E_D t)$$
$$+ B_{R_{-,b}}(\boldsymbol{p}) \exp[-\Delta M_B(T-t)], \quad (3.13)$$

and for the time dependence of $\boldsymbol{x}_f(\boldsymbol{p},t,T)$, we use the same form, except replacing ΔM_B with ΔM_D.

TABLE III.   Comparison of ground-state energies E_D, excited-state energies E'_D, and ground-state overlap factors Z_d and Z_{1S} for the $(2+2)$-state and $(3+3)$-state two-point-correlator fits for the D meson on the $a \approx 0.12$ fm, $\hat{m}' = 0.14 m'_s$ ensemble. In all cases the $(2+2)$-state fitting range is [6, 16] and the $(3+3)$-state fitting range is [4, 23]. We use $(3+3)$-state fits for the analysis; the $(2+2)$-state fits just provide a check of systematic effects.

	Ground state (aE_D)		First excited state (aE'_D)				χ^2/df	
p $(2\pi/L)$	$2+2$	$3+3$	$2+2$	$3+3$	$Z_{1S,1S}$	$Z_{d,d}$	$2+2$	$3+3$
000	0.9566(6)	0.9566(7)	1.54(3)	1.41(4)	4.045(29)	0.0785(7)	18.9/18	35.5/37
100	1.0013(10)	1.0017(9)	1.55(2)	1.39(4)	2.912(36)	0.0741(10)	16.5/18	46.6/37
110	1.0436(15)	1.0433(12)	1.56(2)	1.41(3)	2.149(38)	0.0704(13)	16.5/18	36.9/37
111	1.0838(21)	1.0831(15)	1.60(2)	1.45(3)	1.628(40)	0.0673(18)	22.6/18	39.3/37
200	1.1206(31)	1.1172(23)	1.60(3)	1.48(4)	1.279(46)	0.0658(25)	17.4/18	46.9/37

C. Correlator fitting

We obtain the lattice form factors via a two-step procedure. First, we fit the B- and D-meson two-point correlators to obtain the energies and overlap factors. Then we use these results as constraints with Bayesian priors in the three-point fits. Errors in the resulting form factors h_+ and h_- are determined from a complete single-elimination jackknife procedure.

1. Two-point correlator fits

The two-point functions are constructed from both a local and a smeared interpolating operator. They are fit simultaneously to determine the ground- and excited-state energies. We include oscillating and nonoscillating states in pairs and test the stability of the fits by comparing results with $2+2$ and $3+3$ states. An example is shown in Table III for the $a \approx 0.12$ fm, $\hat{m}' = 0.14 m'_s$ ensemble. For this case we choose a fit range of [4,23] with $3+3$ states. Results for the energy and overlap factor for that range agree with fits in the range [6,16] with $2+2$ states. For the analysis, we use fits with $3+3$ states; the $(2+2)$-state fits provide a check of systematic effects from excited-state contamination. We select approximately the same fit ranges in physical units for all ensembles, as shown in Table IV.

2. Three-point correlator fits

To determine the nonzero-recoil form factor $R_+(\boldsymbol{p})$, we fit three ratios simultaneously: the double ratio for the 1S source from Eq. (3.5) and the local- and smeared-source ratios $Q_{+,d}(\boldsymbol{p},t,T)$ and $Q_{+,1S}(\boldsymbol{p},t,T)$ from Eq. (3.9). Because the fit model [Eq. (3.10)] includes effects of the same first-excited states that occur in the two-point functions, we use the two-point-fit values for these states to set priors for δm, δE_D, and δM_B. The best-fit values are used as the central values and their errors as the widths of the Gaussian priors. As shown in Table IV, the Euclidean time separation between the B- and D-meson interpolating operators is set at approximately 1.5 fm for all ensembles. This separation is sufficient to reduce the last term in Eq. (3.8) to the 10^{-4} level. Fit ranges are chosen for

stability. We use the same range for all three-point correlators in a given ensemble. The ranges are listed in Table IV, and a sample three-point fit is plotted in Fig. 2, left.

For $\boldsymbol{x}_{f,b}(\boldsymbol{p},t,T)$ and $\boldsymbol{R}_{-,b}(\boldsymbol{p},t,T)$, we fit values for both local and smeared sources jointly with the fitting form of Eq. (3.13). Sample three-point fits are plotted in the middle and right panels of Fig. 2. Then, having determined all the needed quantities, we calculate w, $h_+(w)$, and $h_-(w)$ from Eqs. (2.17) and (2.22)–(2.23) for each momentum $\boldsymbol{p}$ and ensemble.

D. Heavy-quark-mass adjustment

We adjust the bare masses of the b and c quarks so that the kinetic masses of the D_s and B_s mesons obtain their physical values. When computing the two-point and three-point correlators, we used good estimates of these quark masses. By the end of the data generation, we could obtain better estimates via the procedure described in [5].

Because there are small differences between the simulation values and final, tuned values, an adjustment of the form factors is required. Details are given in Appendix A. To obtain the adjustment we computed a full set of correlation functions on one of our ensembles with a few heavy-quark masses close to the tuned value and use these results to calculate the slopes of the form factors with respect to the quark masses. These results and the known corrections then give the needed small adjustments

TABLE IV.   Fit ranges $[t_{\min}, t_{\max}]$ for two-point and three-point functions and B-D time separations T. They are chosen to be approximately similar in physical units and independent of sea-quark masses with one exception: for the case $a \approx 0.12$ fm and $\hat{m}'/m'_s = 0.1$, the two-point range was [3,23].

$\approx a$ (fm)	D-meson two-point	B-meson two-point	three-point	T
0.12	[4,23]	[4,15]	[2,10]	12,13
0.09	[5,33]	[9,24]	[2,15]	17,18
0.06	[7,45]	[8,32]	[4,18]	24,25
0.045	[11,80]	[8,32]	[7,24]	32,33

TABLE V. One-loop estimates of the matching factors for the lattice ensembles in this study. Shown are the approximate lattice spacing in fm, the sea-quark mass ratio $\hat{m}'/m'_s$, the tuned κ values of the charm and bottom quarks [5], the strong coupling in the V-scheme evaluated at $q^* = 2/a$, and the zero-recoil factors $\rho_{V^4}(1)$ and $\rho_{V^i}(w)/\rho_{V^4}(w)$ on that ensemble. The first error in each tuned κ value is statistical, and the second reflects the uncertainty in the lattice scale determination [5]. The correction factors are evaluated at the tuned heavy-quark masses except for ρ_{V^i}/ρ_{V^4}, which is evaluated at $m_c a = 0$. The systematic uncertainties in the ρ factors are discussed in Sec. IV and Appendix B.

$\approx a$ (fm)	$\hat{m}'/m'_s$	κ_c	κ_b	$\alpha_V(q^* = 2/a)$	$\rho_{V^4}(1)$	$\rho_{V^i}(w)/\rho_{V^4}(w)$
0.12	0.4	0.12452(15)(16)	0.0879(9)(3)	0.3047	1.025105	0.892347
0.12	0.2	0.12423(15)(16)	0.0868(9)(3)	0.3108	1.026472	0.888051
0.12	0.14	0.12423(15)(16)	0.0868(9)(3)	0.3102	1.026395	0.888248
0.12	0.1	0.12423(15)(16)	0.0868(9)(3)	0.3102	1.026388	0.888241
0.09	0.4	0.12737(9)(14)	0.0972(7)(3)	0.2582	1.015603	0.924664
0.09	0.2	0.12722(9)(14)	0.0967(7)(3)	0.2607	1.016080	0.923051
0.09	0.15	0.12718(9)(14)	0.0966(7)(3)	0.2611	1.016160	0.922757
0.09	0.1	0.12714(9)(14)	0.0965(7)(3)	0.2619	1.016259	0.922319
0.09	0.05	0.12710(9)(14)	0.0964(7)(3)	0.2623	1.016340	0.922022
0.06	0.4	0.12964(4)(11)	0.1054(5)(2)	0.2238	1.008792	0.947870
0.06	0.2	0.12960(4)(11)	0.1052(5)(2)	0.2245	1.008945	0.947361
0.06	0.14	0.12957(4)(11)	0.1051(5)(2)	0.2249	1.009017	0.947085
0.06	0.1	0.12955(4)(11)	0.1050(5)(2)	0.2253	1.009098	0.946829
0.045	0.2	0.130921(16)(70)	0.1116(3)(2)	0.2013	1.004566	0.962520

tabulated in Table XII. The size of the heavy-quark mass corrections to h_+ (h_-) range from 0 to 0.2% (0 to 2%). Small errors arise both from uncertainties in the tuned quark masses and uncertainties in the determination of the slopes.

E. Current renormalization

Here we summarize the procedure for matching the lattice matrix elements to the continuum. The three-point fits yield ratios in which the flavor-diagonal factors $Z_{V^4_{cc}} Z_{V^4_{bb}}$ from Eq. (2.11) cancel. Thus, to normalize the form factors to continuum conventions, we only have to apply the flavor off-diagonal factors ρ_{V^μ} as in Eqs. (2.18)–(2.20). Matching factors with two heavy quarks depend on the recoil w, but the w dependence is not available. Even so, we can obtain some information by considering the limit $m_{2c} a \ll 1$, where the w dependence goes away. For this reason, each of the matching factors in Eqs. (2.18)–(2.20) requires somewhat different treatment. Appendix B provides further details on the matching calculations.

The calculation of the zero-recoil matching factor $\rho_{V^4}(1)$ needed to renormalize R_+ is completely analogous to that of the axial-vector matching factor used in Ref. [5]. Following Ref. [19], we compute it to one-loop order in perturbation theory,

$$\rho_{V^4}(1) = 1 + \alpha_V(q^*)\rho_{V^4}^{[1]}(1), \qquad (3.14)$$

where $\alpha_V(q^*)$ is the QCD coupling in the V scheme [43], evaluated here at the scale $q^* = 2/a$. The result for each ensemble is listed in Table V.

For the matching factor $\rho_{V^4}(w)/\rho_{V^4}(1)$, we note that, by construction, the one-loop coefficient must be proportional to $w - 1$. Moreover, for $m_{2c} a \ll 1$, which holds on the two finest lattices, one may treat the charm quark as a light quark [19], using the HQET formalism for heavy-light currents [44]. The w dependence goes away in this limit, so the one-loop coefficient must also be proportional to $m_{2c} a$. Thus, $\rho_{V^4}(w)/\rho_{V^4}(1) = 1 + \mathcal{O}(\alpha_s(w-1)m_{2c}a)$, where the coefficient of the one-loop correction is not known. In our analysis, we take $\rho_{V^4}(w)/\rho_{V^4}(1) = 1$ and include the estimated size of the one-loop correction as a w-dependent uncertainty.

For the matching factor $\rho_{V^i}(w)/\rho_{V^4}(w)$, we can take the heavy-light theory a step further and calculate the matching explicitly for $m_{2c} a \ll 1$. The calculation does not depend on w. The resulting values for $\rho_{V^i}(w)/\rho_{V^4}(w)$ as in Eq. (3.14) are listed in Table V. The error in the one-loop coefficient introduced by taking the limit $m_{2c} a \to 0$ is proportional to $\alpha_s m_{2c} a$ with a, presumably, mild w dependence, and is again included as an uncertainty.

F. Chiral-continuum extrapolation

The resulting form factors h_+ and h_-, after applying the κ corrections and renormalization factors, are shown in Fig. 3. As can be seen, the dependence of h_+ on lattice spacing a and light-quark-mass ratio $\hat{m}'/m'_s$ is quite mild. The form factors must be extrapolated to the physical average value of the up and down quark mass $r_1\hat{m}$ and zero lattice spacing ($a \to 0$) (the physical point).

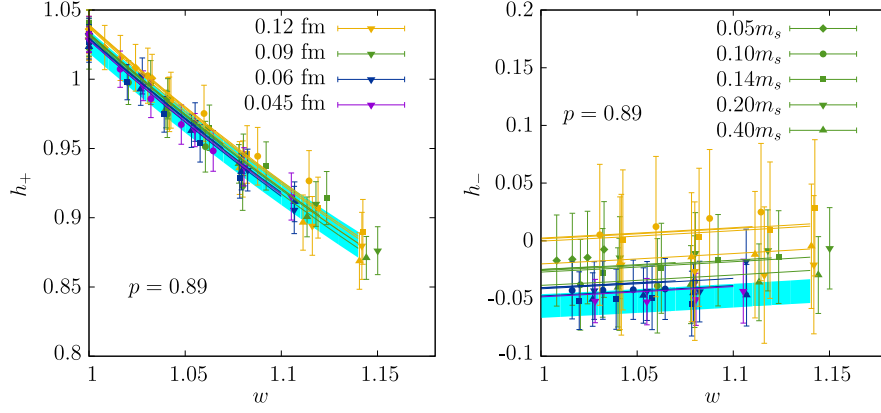To this end we fit both form factors to the following expressions:

FIG. 3 (color online).   Global fit of all data for the form factors h_+ (left) and h_- (right) vs recoil w. The blue (shaded) band gives the 1σ confidence range for the continuum extrapolation at physical quark masses. Fit errors include statistics, matching, and truncation of the chiral expansion. The legend in the left figure gives the color convention for the lattice spacing, and, in the right, it gives the shape convention for the sea-quark mass ratio.

$$h_+(a, \hat{m}', m'_s, w) = 1 + \frac{X_+(\Lambda_\chi)}{m_c^2} - \rho_+^2(w-1) + k_+(w-1)^2 + c_{1,+}x_l + c_{a,+}x_{a^2} + c_{a,a,+}x_{a^2}^2$$

$$+ c_{a,m,+}x_l x_{a^2} + c_{2,+}x_l^2 + \frac{g_{D^*D\pi}^2}{16\pi^2 f_\pi^2 r_1^2}\text{logs}_{\text{SU(3)}}(a, \hat{m}', m'_s, w, \Lambda_\chi), \tag{3.15}$$

$$h_-(a, \hat{m}', m'_s, w) = \frac{X_-}{m_c} - \rho_-^2(w-1) + k_-(w-1)^2 + c_{1,-}x_l + c_{a,-}x_{a^2} + c_{a,a,-}x_{a^2}^2 + c_{a,m,-}x_l x_{a^2} + c_{2,-}x_l^2, \tag{3.16}$$

which contain the correct dependence on the light and strange-quark masses, lattice spacing, and recoil w at next-to-leading order (NLO) in chiral perturbation theory. The chiral logarithm term, denoted "logs$_{\text{SU(3)}}$," contains non-analytic dependence upon the pion and kaon masses (or equivalently $\hat{m}'$ and m'_s). It comes from a staggered-fermion version of the one-loop continuum result of Chow and Wise [45] that includes taste-breaking discretization effects [46]. The explicit expression for logs$_{\text{SU(3)}}$ is given in the appendix of Ref. [15]. The coefficient of the logarithm term is predicted in χPT, but depends upon the value of the D^*-D-π coupling, $g_{D^*D\pi}$, which is not known precisely. We allow $g_{D^*D\pi}$ to vary in the fit, but constrain it with a Gaussian prior 0.53 ± 0.08, motivated by the spread of experimental [47–49] and recent lattice-QCD results [50–55]. The analytic terms depend on the light spectator-quark mass through $x_l = 2B_0\hat{m}'/(8\pi^2 f_\pi^2)$ and on the lattice spacing through $x_{a^2} = [a/(4\pi f_\pi r_1^2)]^2$, which, according to χPT power counting, are expected to have coefficients of order 1 [40]. The NLO expression is supplemented by next-to-next-to-leading order (NNLO) analytic terms in the light-quark mass $\hat{m}'$ and lattice spacing to incorporate the error from the truncation of the chiral expansion, as explained below, and by terms analytic in $(w-1)$ to allow interpolation in w at nonzero recoil. We do not include analytic functions of the strange sea-quark mass because

(1) we do not have sufficiently varied values of m'_s to be able to resolve any strange-quark mass dependence, (2) from χPT we expect the sea-quark mass dependence of the form factors to be significantly smaller than the light spectator-quark mass dependence, and (3) as discussed in Sec. IV G, we do not observe any strange sea-quark mass dependence within our current statistical precision.

The statistical errors and correlations from the two-point and three-point ratio fits are propagated to the chiral fits using a single-elimination jackknife procedure. The strongest correlations are between the data for $h_+(w)$ [or $h_-(w)$] at different w values on the same ensemble. The data for $h_+(w)$ and $h_-(w)$ on the same ensemble are only weakly correlated. Results from different ensembles are statistically independent. The fits to Eqs. (3.15) and (3.16) are done taking fully into account all statistical correlations.

To test the applicability of NLO chiral perturbation theory to our data, we first fit without the analytic NNLO terms. The p value, $p = 0.93$ of the joint, exclusively NLO fit to h_+ and h_- is satisfactory.[1] Next we

---

[1]With Gaussian priors our p value is determined from the augmented χ^2. We count degrees of freedom as the number of data points minus adjustable parameters plus the number of theoretically motivated priors. Very loose priors that have no impact but to stabilize the fits are not counted.
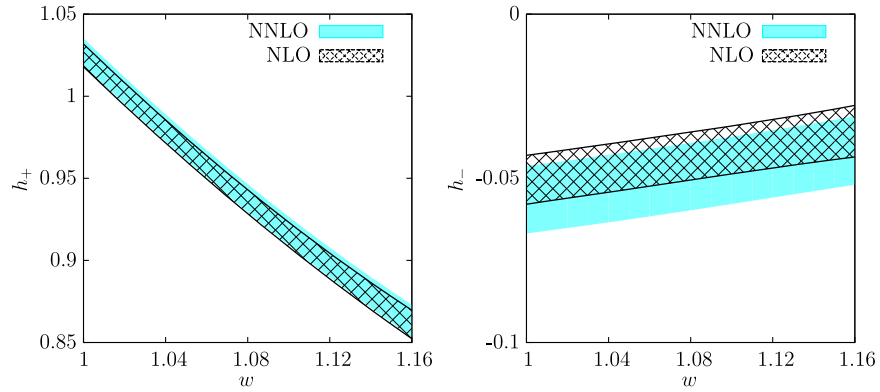
FIG. 4 (color online).   Comparison of NLO (hatched) and NNLO (solid) chiral-continuum fits for h_+ (left) and h_- (right) vs recoil w.

include the analytic NNLO terms with priors 0 ± 2 based on expectations from χPT power counting in order to test for the effect of truncating the chiral perturbation series. The p value decreases slightly to 0.87. Including these terms increases the standard deviation by at most $\sim$10% for h_+ and $\sim$30% for h_-, and shifts the central values by much less than the final standard deviation, as shown in Fig. 4. The statistical errors then can be safely assumed to include the systematic error of the truncation. We therefore use this fit including NNLO terms to obtain our preferred value for the form factors at the physical point. The results of the extrapolation with propagated statistical errors are shown as bands in Fig. 3.

In heavy-quark effective theory, Luke's theorem states that $h_+(w = 1)$ has leading corrections only at second order in the inverse heavy-quark masses, namely, $1/m_c^2$ and $1/m_b^2$, whereas h_- has corrections at first order. Appendix B and Ref. [56] show how Luke's theorem applies in lattice gauge theory and, hence, that one expects h_- to have larger heavy-quark discretization errors than h_+. Indeed, we see that h_- does have a stronger dependence on lattice spacing than h_+. For the determination f_+, and therefore $|V_{cb}|$, the contribution of h_- over the entire kinematic range is small, so the larger errors in h_- do not increase the overall error much. These trends in lattice spacing with 14 ensembles are consistent with our previous findings with 4 ensembles [15].

We build the systematic errors from κ tuning and from the matching factors into the chiral-continuum extrapolation by forming the combined covariance matrix for the data as follows:

$$C_{ij} = C_{ij}^{\text{stat}} + \delta_i^{(\rho)}\delta_j^{(\rho)} + \delta_i^{(\kappa)}\delta_j^{(\kappa)}, \qquad (3.17)$$

where the first term is the statistical covariance, and the index i runs over all data (ensembles, momenta, and h_+ and h_-). We denote by $\delta_i^{(\rho)}$ and $\delta_i^{(\kappa)}$ the shift on the ith datum due to the matching and κ-tuning errors, respectively. Equation (3.17) conservatively assumes that the matching-factor errors (or κ-tuning errors) are 100%

correlated between all data points. For the systematic errors due to our matching procedure, we have estimates for the uncertainty in $\rho_{V^4}(1)$, $\rho_{V^4}(w)/\rho_{V^4}(1)$ and $\rho_{V^i}(w)/\rho_{V^4}(w)$ in Eqs. (B31), (B29), and (B37), respectively. The form factors $h_\pm(w)$ change the most when $\rho_{V^4}(w)$ and $\rho_{V^i}(w)/\rho_{V^4}(w)$ are simultaneously shifted in opposite directions. We take the average of these two shifts as an estimate of the ρ-factor error for all $h_\pm(w)$ on all ensembles. For the κ-tuning error, we take the same approach in principle, propagating the uncertainties of the intercepts and slopes in Appendix A to shifts $\delta_i^{(\kappa)}$ of the form-factor data. However, we find that the resulting $\delta_i^{(\kappa)}$ are negligibly small, and we therefore set them to zero in Eq. (3.17).

Given the chiral-continuum fit results for h_+ and h_-, we construct the vector and scalar form factors f_+ and f_0 using Eqs. (2.5) and (2.6). Figure 5 compares our new $B \to D\ell\nu$
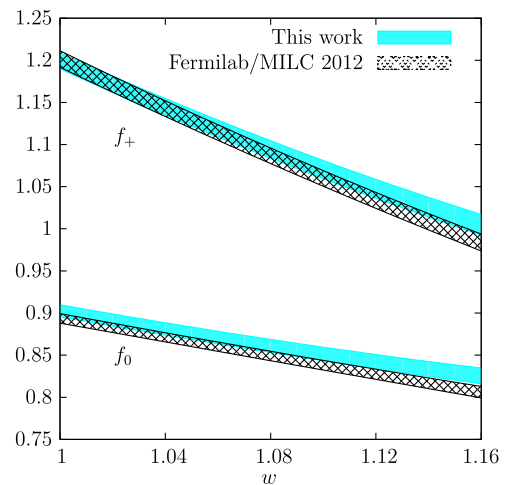

FIG. 5 (color online).   The form factors f_+ and f_0 as a function of the recoil w resulting from the chiral-continuum fit in this study (cyan band), compared with the results from [15] (cross-hatched band). The width of each band indicates the 1σ error from the chiral-continuum fit, but uncertainties from the matching factors are included only in the cyan bands. See the text for additional details.
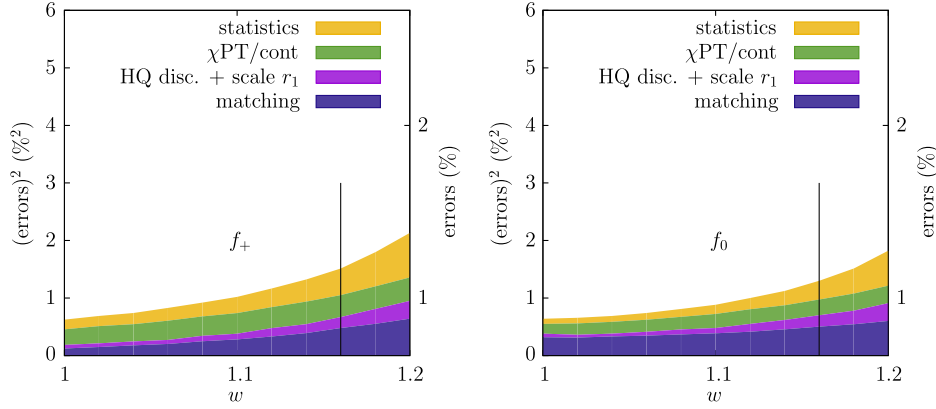
FIG. 6 (color online).   Error budgets for f_+ and f_0 as a function of the recoil w. The colored bands show the error contribution of each uncertainty source to the quadrature sum. The corresponding error is provided on the right y axis. Our lattice simulation results are for $w \in [0, 1.16]$, i.e., to the left of the vertical line.

form-factor results with those from our earlier work [15] in the w range where we have simulation data. The curves shown are output from the chiral-continuum extrapolation, and therefore include the uncertainties from statistics, the chiral-continuum extrapolation, and matching (for the current work); they do not include the remaining systematic uncertainties, which we add in quadrature *a posteriori* in both works. We expect that the two results are largely independent because they have only a small subset of overlapping data (the earlier work included only four ensembles), and the new work includes NNLO analytic terms in the χPT fit function. The results are consistent for both form factors over almost all simulated w values, and diverge only slightly for f_0 for $w > 1.13$. The central values of the new form factors are slightly higher than in [15], primarily due to explicit inclusion of the perturbative correction factors $\rho_{V^i}(w)/\rho_{V^4}(w)$ which have a bigger effect on the form factor f_0 than on f_+. The total errors on the form factors in this work are similar in size to those in Ref. [15], but the additional ensembles used in this work enable a more detailed and reliable systematic error analysis as described in Sec. IV. (Reference [15] focused on form-factor ratios in which most of the systematic errors are suppressed.)

IV. SYSTEMATIC ERRORS

In this section we discuss the sources of systematic error in the lattice determinations of h_+ and h_- and their propagation to the form factors f_+ and f_0. As can be seen from Fig. 4, the magnitude of h_- is about 5% of h_+ for the entire range of simulated w values. Further, the contribution of h_- to the vector form factor f_+ is suppressed relative to the contribution from h_+ by the factor $(1 - r)/(1 + r) =$ 0.477, while the contribution of h_- to the scalar form factor f_0 is exactly zero at $w = 1$ and grows linearly with recoil as $(w - 1)$. Thus even large percentage systematic

errors in h_- lead to only small uncertainties in f_+ and f_0. Figure 6 shows the momentum dependence of the error contributions to $f_+(w)$ and $f_0(w)$, while Table VI provides numerical values for a representative recoil $w = 1.16$.

A. Overview of systematic errors in f_+ and f_0

As can be seen from Fig. 6, the dominant uncertainty in both form factors arises from the chiral-continuum fit, which includes contributions from statistics, matching factors, and higher-order terms in the chiral expansion. Although we cannot strictly disentangle the contributions to the error from these sources, we can estimate their sizes by repeating the chiral-continuum fit omitting either the errors in the matching factors or the NNLO terms in the chiral expansion, and take the quadrature difference of

TABLE VI.   Error budget (in percent) for f_+ and f_0 at $w = 1.16$, which is the largest recoil value used in our momentum extrapolation to the full kinematic range and determination of $|V_{cb}|$ (see Sec. V). The first row includes the combined error from statistics, matching, and the error from truncating the chiral expansion resulting from the chiral-continuum fit: errors in parentheses are approximate subparts estimated as described in the text. The total error is obtained by adding the individual errors in quadrature. Not explicitly shown because they are negligible are finite-volume effects, isospin-breaking effects, and light-quark mass tuning.

Source	$f_+(\%)$	$f_0(\%)$
Statistics + matching + χPT cont extrap.	1.2	1.1
(Statistics)	(0.7)	(0.7)
(Matching)	(0.7)	(0.7)
(χPT/cont extrap.)	(0.6)	(0.5)
Heavy-quark discretization	0.4	0.4
Lattice scale r_1	0.2	0.2
Total error	1.2	1.1

the resulting error estimates. The contribution from "statistics" is defined to be the error in the NLO chiral-continuum fit to data with no matching-factor uncertainties included. This imprecise scheme does not guarantee that the individual errors sum to the total fit error, but, roughly speaking, we find that the statistics, matching, and truncation uncertainties in the chiral-continuum expansion contribute approximately equally to the error in the full NNLO fit. Despite our incomplete knowledge of the matching factors, we find their contributions to the uncertainty in f_+ and f_0 to be modest. The errors from the chiral-continuum fit are under good control for the range of simulated lattice recoil values, but grow rapidly for $w \gtrsim 1.16$ where we do not have data.

We add the remaining systematic uncertainties *a posteriori* to the chiral-continuum fit error. We estimate the individual contributions to the form-factor error budget in the following subsections, discussing each source in a separate subsection for clarity. In practice, only the heavy-quark discretization errors (Sec. IV D) and lattice-scale uncertainty (Sec. IV E) turn out to be significant.

We assume that systematic uncertainties from heavy-quark discretization effects and the lattice-scale uncertainty are uncorrelated, and therefore add them in quadrature. We then propagate them to f_+ and f_0 according to the linear transformation Eqs. (2.5) and (2.6), which depends on the recoil w, taking them to be 100% correlated between w values and between h_+ and h_-. Both the lattice-scale and heavy-quark discretization errors are substantially smaller than the chiral-continuum fit error, and increase only slowly with w.

B. Matching

The ρ factors in Eq. (2.11) enter in the renormalization of the components of the transition vector current V_{cb}^μ. As explained in Sec. III E these factors are estimated in one-loop lattice perturbation theory to the extent that such calculations are available. As discussed near the end of Sec. III F, we build the uncertainty estimates of Eqs. (B31), (B32), and (B37) into the chiral-continuum fit via Eq. (3.17).

A noteworthy feature of Table VI is the size of the matching error after the chiral-continuum fit. Had we omitted the errors in Eqs. (B31), (B32), and (B37) from the fitting function, we would have to add them *a posteriori*, as we did for $B \to D^*$ at zero recoil [5]. Following the procedure used in Ref. [5], we would assign errors of 1.4% and 1.1% for f_+ and f_0, respectively, at $w = 1.16$, based on the second-finest lattice with $a \approx 0.06$ fm and its value of $\alpha_s = 0.225$. Incorporating the matching errors into the chiral-continuum fit, however, allows them to vary with lattice spacing and to be informed by the data. It is reasonable that the additional information reduces the uncertainty to about 0.7% for both f_+ and f_0 at $w = 1.16$, as shown in Table VI.

C. Light-quark and gluon discretization errors

Our improved actions have light-quark and gluon discretization errors of order $\alpha_s a^2$ and $\alpha_s^2 a^2$ [5]. As discussed in Sec. III F, they are already included in the fit model of Eqs. (3.15) and (3.16). From Table VI, the errors due to the truncation of the chiral expansion and extrapolation to the continuum limit are about 0.6% and 0.5% for f_+ and f_0, respectively, at $w = 1.16$. Using simple power-counting, we would conservatively estimate the size of generic light-quark and gluon discretization errors on the $a \approx 0.06$ fm lattice to be about 1%. The data for h_+, which give the dominant contribution to f_+ and f_0, do not display significant lattice-spacing dependence. Therefore, allowing the data to constrain the possible size of light-quark and gluon discretization effects reduces the error.

D. Heavy-quark discretization errors

An important uncertainty comes from discretization errors in the lattice treatment of the heavy quarks. Applying the theory of heavy-quark cutoff effects developed in Refs. [19,56], we estimate the size of these errors in Appendix B, providing in Tables XIII and XIV numerical results for the errors on $h_\pm(w)$ from mismatches in the lattice action and currents for a heavy-quark scale of $\bar\Lambda = 450$ MeV. The value is the same as that used in Ref. [5], and here we explain why this choice is reasonable in this case too.

In Fig. 7, we show the observed lattice-spacing dependence of our simulation data for $h_+(w)$ at three recoil values on the $\hat m' = 0.2m'_s$ ensembles. The raw data (black squares) are adjusted slightly to obtain the same w values for all a using a chiral-continuum fit with the ρ-factor and κ-tuning errors turned off. Thus, the error bars shown here are statistical only. We also use this fit to adjust the light-quark masses to those on the $\hat m' = 0.2m'_s$, $a \approx 0.09$ fm ensemble (orange circles). (In practice, shifting the strange sea-quark mass has little impact on the fit points.) To compare the trend with the expected heavy-quark discretization error, we draw the size of the effect—defined as the difference from $a \approx 0.09$ fm—predicted in Appendix B for $\bar\Lambda = 450$ MeV.

For all values of w, Fig. 7 shows that this estimate captures most of the discretization effect, given the statistical scatter. Note that the fit-interpolated (orange) points make clear that the trend is predominantly linear in a^2. This dependence is characteristic of generic discretization effects of the light quarks and gluons, which are already included in the chiral-continuum fit model, Eqs. (3.15) and (3.16). Moreover, the heavy-quark discretization effects turn out to be nearly linear in a^2, so they, too, are mostly absorbed by the fit model. It does not make sense to count this well-modeled a dependence twice by, say, inflating $\bar\Lambda$ to encompass all of the variation seen in Fig. 7. That said, we do not have an argument to reduce the value of $\bar\Lambda$ used in
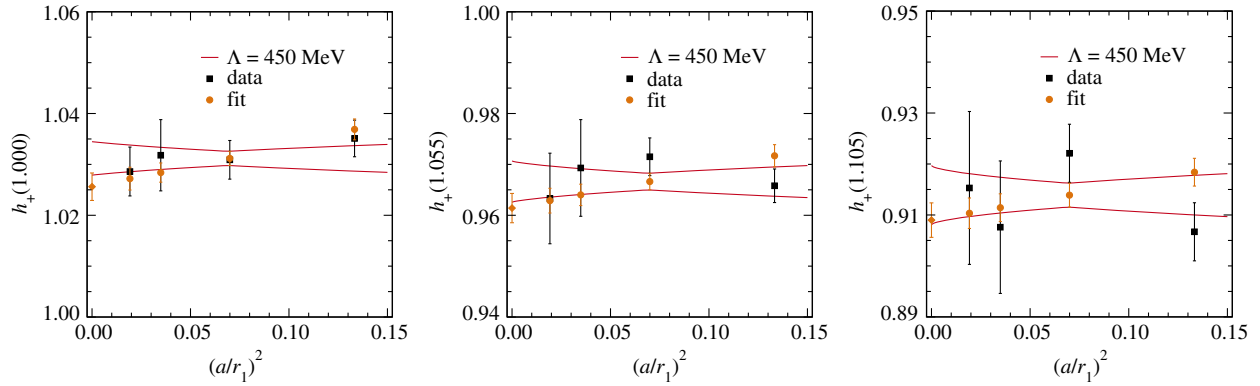
FIG. 7 (color online). The form factor $h_+(w)$ at three representative values of the recoil w as a function of the squared lattice spacing $(a/r_1)^2$, for all ensembles with $\hat{m}' = 0.2m'_s$. Black squares denote data points interpolated to the same recoil value, while orange circles denote fit values interpolated further, so that the light-quark masses $\hat{m}'$ and m'_s correspond to the values on the lattice with $a \approx 0.09$ fm; the orange diamonds denote the continuum limit in this case. The solid curves show the a dependence predicted by the HQET description of cutoff effects, with $\bar{\Lambda} = 450$ MeV. These trends are shown as deviations from the $a \approx 0.09$ fm lattice. For details, see the discussion of Tables XIII and XIV in Appendix B. Note that the data and fit points reflect discretization errors from light quarks and gluons, as well as those from the heavy quarks.

Tables XIII and XIV below 450 MeV. Following Ref. [5], we base our final estimate on our next-to-smallest lattice spacing, $a \approx 0.06$ fm, leading to the error estimates in Table VI. The heavy-quark discretization error is found to be small compared with the chiral-continuum extrapolation error. For $h_+(w)$ it ranges from approximately 0.15% at $w = 1$ to 0.35% at our largest w values. For $h_-(w)$ it is approximately 20%.

E. Lattice-scale error

We use the distance scale r_1 and the relative lattice spacing a/r_1 to determine the lattice scale a. The ratio a/r_1 for the ensembles in this study is known quite precisely from a fit to a wide range of data for the heavy-quark potential [23]. For this study we use the values of r_1/a presented in Table III of [5]. The continuum, physical quark-mass value of r_1 is determined from studies of the light pseudoscalar-meson spectrum and decay constants. For this study we use $r_1 = 0.3117(22)$ fm, based on the PDG value of f_π [40].

Because the form factors are dimensionless, the lattice scale enters only weakly into their determination via (1) tuning the heavy-quark masses, (2) setting light-meson masses in the chiral logarithms, and (3) fixing the location of the continuum limit. To determine the error due to uncertainties in r_1 we see how much our results shift when we change r_1 by one standard deviation. We find that the changes in the form factors are smaller than 0.2%.

F. Finite-volume corrections

The finite-volume effects can be estimated within NLO heavy-light meson χPT by replacing the loop integrals with discrete sums. The corrections to the integrals in the formulas appearing in $B \to D$ decays at zero recoil were worked out by Arndt and Lin [57]. At the values of quark masses and volumes at zero recoil where we have data, the effects predicted by χPT are less than one part in 10^4. This is not a result of cancellation, but is due to the fact that the chiral logarithms make only a very small contribution to the form factor. We did not calculate the finite-volume corrections at nonzero recoil because the integrals appearing in those formulas are much more complicated, but there is no reason to expect these effects to be significantly enhanced away from the zero-recoil point. Thus, finite-size effects are expected to be negligible compared with our other errors, and we do not assign any additional error due to them.

G. Light-quark-mass tuning

We extrapolate the form factors to the physical average of the up- and down-quark masses $r_1\hat{m} = 0.003612(126)$, determined from an analysis of the light pseudoscalar-meson spectrum and decay constants on the same ensembles [58]. Varying $r_1\hat{m}$ by plus and minus 1σ in our chiral-continuum fit leads to relative changes of order 10^{-5} for both form factors in the range of simulated recoil values.

On some ensembles the strange sea-quark mass deviates by as much as 30% from its physical value. From heavy-light meson χPT, we expect the $B \to D$ form factors to be largely insensitive to sea-quark masses. Nevertheless we study the impact of the strange sea-quark mass by calculating the ratios in Eqs. (2.12)–(2.15) on an $a \approx 0.12$ fm ensemble with an unphysically light strange sea quark, $a\hat{m}'/am'_s = 0.005/0.005$. We do not observe any statistically significant differences in these ratios from those on the $a\hat{m}'/am'_s = 0.005/0.05$ ensemble. We therefore conclude that errors from mistuning the strange sea-quark mass are negligible within our current precision.

TABLE VII.   Selected values of the form factors $f_+(w)$ and $f_0(w)$ at the physical point (synthetic data) and their correlations. Errors shown include statistics and all systematics added in quadrature.

	Value	Correlation matrix					
		$f_+(1)$	$f_+(1.08)$	$f_+(1.16)$	$f_0(1)$	$f_0(1.08)$	$f_0(1.16)$
$f_+(1)$	1.1994(095)	1.0000	0.9674	0.8812	0.8290	0.8533	0.8032
$f_+(1.08)$	1.0941(104)		1.0000	0.9523	0.8241	0.8992	0.8856
$f_+(1.16)$	1.0047(123)			1.0000	0.7892	0.8900	0.9530
$f_0(1)$	0.9026(072)				1.0000	0.9650	0.8682
$f_0(1.08)$	0.8609(077)					1.0000	0.9519
$f_0(1.16)$	0.8254(094)						1.0000

H. Heavy-quark-mass tuning

As described in Sec. III D, we adjust the simulation data before the chiral-continuum fit to account for the slight difference between the simulated bottom and charm κ values and the physical ones, using the corrections estimated in Appendix A. The size of these corrections is quite small, ranging from 0% to 0.2% for h_+, and from 0% to 2% for h_-. Repeating the chiral-continuum fit omitting the κ corrections does not appreciably change the chiral-continuum fit result. Thus we conclude that the uncertainty in the form factors due to errors in the heavy-quark masses is negligible.

I. Isospin correction

In our calculation we have assumed that the up- and down-quark masses are equal, although in Nature, they are not. Therefore, if we distinguish between them in calculating the value of the form factors at the physical point, we get a slightly different result. To estimate the sensitivity of f_+ and f_0 to isospin splitting of the light-quark masses, we use our best-fit parameters in the chiral-continuum model, and evaluate the fit function at the physical values of $r_1 m_u = 0.002236$ and $r_1 m_d = 0.004988$, instead of $r_1 \hat{m}$ given above. These values are obtained by combining $r_1 \hat{m}$ obtained on the asqtad ensembles with the ratio $m_u/m_d = 0.4482(^{+173}_{-207})$ obtained from the MILC Collaboration's study of electromagnetic effects on the pion and kaon mass splittings on the $(2+1+1)$-flavor HISQ ensembles [59]. The relative shifts in both form factors for all simulated recoil values are of order 10^{-4}, and therefore negligible. Although this method varies the light valence- and sea-quark masses together, the shifts are primarily due to the different valence-quark mass.

V. DETERMINATION OF $|V_{cb}|$

A. Synthetic data

The preferred chiral-continuum fit results for $h_+(w)$ and $h_-(w)$ are continuous functions of w at zero lattice spacing and physical quark masses. Via Eqs. (2.5) and (2.6), we can obtain the corresponding functions for $f_+(w)$ and $f_0(w)$. As discussed above, the errors are under control for $w < 1.2$, i.e., where we have lattice measurements. Following Refs. [15,42], we proceed to extend our results to the full kinematic range by generating synthetic data $f_+(w_j)$ and $f_0(w_j)$ for a finite set of w values, w_j. Because the functions are described by only six independent functions (in the physical limit), we can only generate six such data points. Generating more would just lead to a covariance matrix of low rank. We choose the values of $w_j = 1$, 1.08, and 1.16, for f_+ and f_0, to cover the kinematic range of the lattice-QCD calculation. The values of $f_+(w_j)$ and $f_0(w_j)$, as well as the matrix of correlations among them, are given in Table VII.

B. z expansion

Experimental measurements of the form factor are available over a larger kinematic range of w [1, 1.58] than the lattice values [1,1.16], but experimental errors are largest where lattice errors are small and vice versa. Although the value of f_+ at a single w-value suffices for obtaining $|V_{cb}|$, a better strategy is to fit both sets of data simultaneously to a common fitting function in which $|V_{cb}|$ is a free parameter that multiplies all the lattice values and is determined in the fit [15,42]. This approach minimizes the uncertainty in $|V_{cb}|$ by combining all of the available experimental and lattice information. Further, a comparison of the shapes of the experimental and lattice results as a function of w provides a valuable consistency check that is not available when using only a single recoil point.

For this purpose we need a model-independent parametrization to carry out the necessary interpolation/extrapolation. The z expansion of Boyd, Grinstein, and Lebed (BGL) [12] is just such a parametrization. It builds in constraints from analyticity and unitarity. It is based on the conformal map

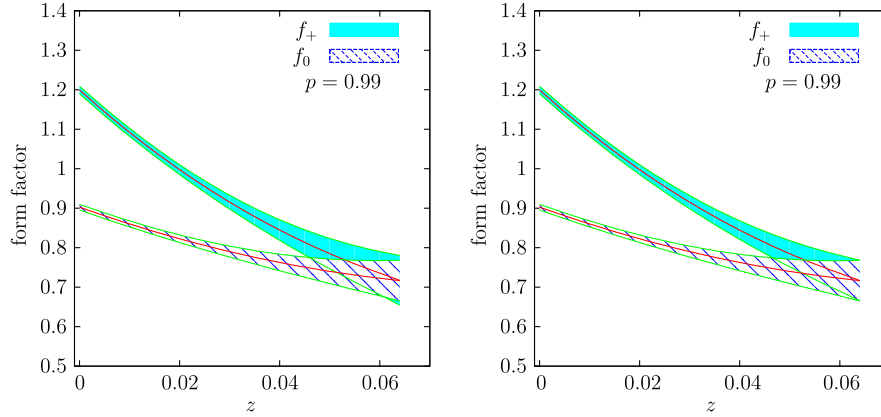$$z(w) = \frac{\sqrt{1+w} - \sqrt{2}}{\sqrt{1+w} + \sqrt{2}}, \qquad (5.1)$$

FIG. 8 (color online).   Result of the z-expansion fit of the lattice form-factor values without (left) and with (right) the kinematic constraint $f_+(q^2 = 0) = f_0(q^2 = 0)$. The expansion is truncated after the cubic term. The solid error band is for f_+, while the slashed band is for f_0. Without imposing the constraint, we find that it is nonetheless satisfied to a high accuracy.

which takes the physical region $w \in [1, 1.59]$ to $z \in [0, 0.0644]$. It pushes poles and branch cuts relatively far away to $|z| \approx 1$. Form factors are then parametrized as

$$f_i(z) = \frac{1}{P_i(z)\phi_i(z)} \sum_{n=0}^{\infty} a_{i,n} z^n, \qquad (5.2)$$

where the $P_i(z)$ are the "Blaschke factors" containing explicit poles (e.g., a B_c or B_c^* meson) in the channel variable q^2, and the ϕ_i are the "outer functions," whose purpose is described below. The only unknown parameters are the polynomial coefficients $a_{i,n}$. In this work, we do not introduce any pole, so $P_i(z) = 1.$[2] The choice of outer functions is arbitrary as long as they are analytic functions that do not introduce poles or branch cuts; the ϕ_i just affect the numerical values of the series coefficients, a_i. For f_+ and f_0, we use

$$\phi_+(z) = \Phi_+ (1+z)^2 (1-z)^{1/2}$$
$$\times [(1+r)(1-z) + 2\sqrt{r}(1+z)]^{-5}, \qquad (5.3)$$

$$\phi_0(z) = \Phi_0 (1+z)(1-z)^{3/2}$$
$$\times [(1+r)(1-z) + 2\sqrt{r}(1+z)]^{-4}, \qquad (5.4)$$

such that, numerically, $\Phi_0 = 0.5299$ and $\Phi_+ = 1.1213$ [12]. With this choice, the bound on the series coefficients from unitarity takes a particularly simple form:

$$\sum_{n=0}^{N} |a_{i,n}|^2 \leq 1, \qquad (5.5)$$

---

[2]We have checked that including a pole located at the theoretically predicted B_c^* mass [60] does not appreciably change the z-fit result.

where this bound holds for any N. This bound, in combination with the small range of $|z|$, ensures that only a small number of coefficients is needed to parametrize the form factors over the entire kinematic range to high precision.

To implement the z expansion, we start from the synthetic data for f_+ and f_0 at z values corresponding to $w_j = 1, 1.08,$ and 1.16, choose a truncation N and fit to

TABLE VIII.   Coefficients of the z expansion for fits to the lattice form factors including the kinematic constraint $f_+(q^2 = 0) = f_0(q^2 = 0)$. For completeness, the inferred value and error in $a_{0,0}$ is quoted. We also show the zero-recoil form factor $\mathcal{G}(1)$. The results for different truncations N are virtually identical. The unusually low (augmented) χ^2 comes about because these fits essentially behave like solves. This happens because the kinematic constraint is so nearly perfectly satisfied already at the quadratic level, $N = 2$. Higher-order terms with $N = 3$ and 4 provide no further improvement and, hence, no change. The coefficients of the higher-order terms are constrained with priors with central value zero and width one. These theoretically motivated priors are counted as data in the degrees of freedom (df).

	$N = 2$	$N = 3$	$N = 4$
$a_{+,0}$	0.01262(10)	0.01262(10)	0.01262(10)
$a_{+,1}$	−0.097(3)	−0.097(3)	−0.097(3)
$a_{+,2}$	0.50(14)	0.50(17)	0.50(17)
$a_{+,3}$	$\cdots$	−0.06(90)	−0.06(90)
$a_{+,4}$	$\cdots$	$\cdots$	−0.0(1.0)
$a_{0,0}$	0.01142(14)	0.01142(14)	0.01142(10)
$a_{0,1}$	−0.060(3)	−0.060(3)	−0.060(3)
$a_{0,2}$	0.31(15)	0.31(15)	0.31(15)
$a_{0,3}$	$\cdots$	0.06(91)	0.06(91)
$a_{0,4}$	$\cdots$	$\cdots$	0.0(1.0)
$\mathcal{G}(1)$	1.0541(83)	1.0541(83)	1.0541(83)
χ^2/df	0.1/1	0.0/1	0.0/1

TABLE IX. Central values, errors, and correlation matrix for the parameters of the cubic fit to f_+ and f_0 including the kinematic constraint at $q^2 = 0$.

		Correlation matrix						
	Value	$a_{+,0}$	$a_{+,1}$	$a_{+,2}$	$a_{+,3}$	$a_{0,1}$	$a_{0,2}$	$a_{0,3}$
$a_{+,0}$	001262(10)	1.00000	0.21726	0.07203	0.00387	0.19347	0.15590	−0.00364
$a_{+,1}$	−00969(34)		1.00000	−0.47505	0.25544	0.80946	−0.26302	−0.18212
$a_{+,2}$	050(17)			1.00000	−0.45415	−0.43845	0.85491	0.25116
$a_{+,3}$	−006(90)				1.00000	0.11415	−0.15582	0.21768
$a_{0,1}$	−00597(29)					1.00000	−0.42932	−0.03556
$a_{0,2}$	031(15)						1.00000	−0.06062
$a_{0,3}$	006(91)							1.00000

determine the coefficients $a_{i,n}$ for $n = 0, \ldots, N$. These coefficients are then used to parametrize the form factors over the full kinematic range. We find we need only the first few coefficients in the expansion to obtain a stable fit with a good p value. The kinematic constraint requires $f_+ = f_0$ at $q^2 = 0$ where $z \approx 0.0644$. It is interesting to fit the data without the constraint to see to what extent it is automatically satisfied. The result for $N = 3$ in the left panel of Fig. 8 shows that the data satisfy the constraint much better than our statistics would suggest. Nonetheless, in subsequent fits, we include the constraint to reduce the form-factor errors at $q^2 = 0$. The constraint is imposed by expressing the parameter $a_{0,0}$ in Eq. (5.2) in terms of the other series coefficients. Table VIII shows the series coefficients and goodness of fit obtained for fits of the lattice form-factor data imposing the kinematic constraint with $N = 2$–4. For the fits at cubic and quartic order in the z expansion, we have more parameters than data, but the

unitarity bound in Eq. (5.5) justifies imposing a prior with central value 0 and width 1 on the coefficient(s) of the cubic (and quartic) term(s).

The truncation of the z expansion introduces a possible systematic error. We take this into account by increasing the truncation order until the central values and errors stabilize. At this point, the errors from the fit reflect the truncation error, and do not need to be counted separately. Table VIII shows that the fit has stabilized by quadratic order. We therefore take the cubic fit, shown in the right panel of Fig. 8, as our preferred parametrization. Table IX gives the central values, errors, and normalized correlation matrix for the series coefficients a_i. This information can be used to reproduce our results for $f_+(w)$ and $f_0(w)$ over the full kinematic range, and in particular, in combined lattice-and-experiment fits to obtain $|V_{cb}|$.

Our zero recoil form factor $[\mathcal{G}(1) = 1.0541(83)]$ can be compared with a recent lattice-QCD calculation by Atoui et al. [61]. Their result, $\mathcal{G}(1) = 1.033(95)$ in two-flavor QCD, agrees with our determination within much larger uncertainties. The only previous calculation at nonzero recoil used quenched QCD [13]. Figure 9 compares their result with ours. Although this earlier calculation was performed in quenched QCD, and thus is subject to an unquantifiable systematic due to the omission of sea-quark effects, it uses step scaling [62] to control heavy-quark discretization effects, plus multiple light-quark masses and lattice spacings to control the mild chiral-continuum extrapolation [13]. Thus it is the best calculation so far for $B \to D\ell\nu$ at nonzero recoil. The two calculations agree for all w values, although the slope of $f_+(z)$ is somewhat steeper for the $(2 + 1)$-flavor result reported here.
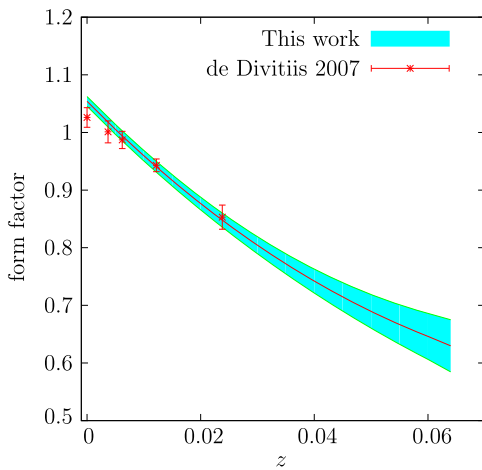

FIG. 9 (color online). Comparison of lattice-QCD results for the $B \to D\ell\nu$ form factor $\mathcal{G}(z)$ at nonzero recoil from this work (curves with error bands) and Ref. [13] (points with error bars). Errors on the data points from Ref. [13] include all uncertainties except for the unquantifiable error due to omitting sea-quark effects.

C. Determination of $|V_{cb}|$

To obtain $|V_{cb}|$, we need lattice results for the form factors and experimental values for $\bar{\eta}_{\text{EW}}|V_{cb}|f_+(w)$. Because the experimental value of the form factor at zero recoil suffers from kinematic suppression, we prefer to fit the theoretical and experimental data over the entire kinematic range. For this work, we use the 2009 B-tagged data from the *BABAR* Collaboration [9], because it is the
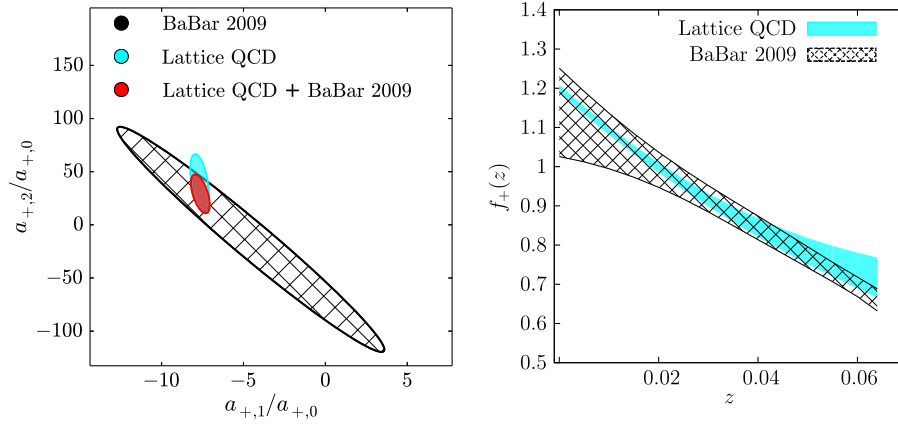
FIG. 10 (color online).   Left: one sigma contour plots showing the correlation between the normalized slope $a_{+,1}/a_{+,0}$ and normalized curvature $a_{+,2}/a_{+,0}$ from $N = 3$ z-expansion fits to either the *BABAR* experimental data alone, our lattice QCD results alone, and a joint fit to both. Right: vector form factor f_+ obtained from separate z-expansion fits of the 2009 *BABAR* experimental data (hatched band) and lattice form factors (solid band).

most precise to date.[3] Reference [9] reports a systematic error of 3.3% at small w. For present purposes, we take 3.3% over the entire kinematic range with 100% correlation and combine this systematic in quadrature with the reported (uncorrelated) statistical errors [63].

Although the *BABAR* Collaboration has applied some radiative corrections to their published data, additional electroweak effects still remain. These include a Sirlin factor for the $W\gamma$ and WZ box diagrams [64] and a further Coulomb correction for final-state interactions in B^0 decays. The *BABAR* Collaboration reports that 37% of the decays in their data sample were B^0s, which results in a QED correction factor in the amplitude of $1 + 0.37\pi\alpha/2$. We have assigned an uncertainty of ± 0.005 to this correction to account for omitted electromagnetic effects at intermediate distances. When combined with the Sirlin factor $\eta_{EW} = 1.00662$ the net electroweak correction becomes $\bar{\eta}_{EW} = 1.011(5)$. [We prefer to use $\mathcal{G}(w)$ to denote the purely hadronic form factor, so in our notation $\bar{\eta}_{EW}|V_{cb}|\mathcal{G}(w)$ corresponds to the quantity often reported as $|V_{cb}|\mathcal{G}(w)$, and the ratio of experimental to theoretical values must be divided by $\bar{\eta}_{EW}$ to get $|V_{cb}|$.]

Before performing a joint fit to the lattice and experimental data, we compare the values of the shape parameters to check for consistency. The left panel of Fig. 10 plots the 1-σ constraints on the curvature $a_{+,2}/a_{+,0}$ versus slope $a_{+,1}/a_{+,0}$ obtained from separate $N = 3$ z-expansion fits of the lattice data and the 2009 *BABAR* experimental data. The results are consistent, but the lattice data constrains the shape much better: this is both because the lattice points are very precise at low recoil, and because they are

---

[3]The Belle experiment presented preliminary measurements of $\bar{\eta}_{EW}|V_{cb}|f_+(w)$ at ICHEP 2014 [10]. Once these are finalized, our form-factor coefficients from Table IX can be used to update $|V_{cb}|$ from a joint lattice-experiment fit with both the Belle and *BABAR* data (including experimental correlations).
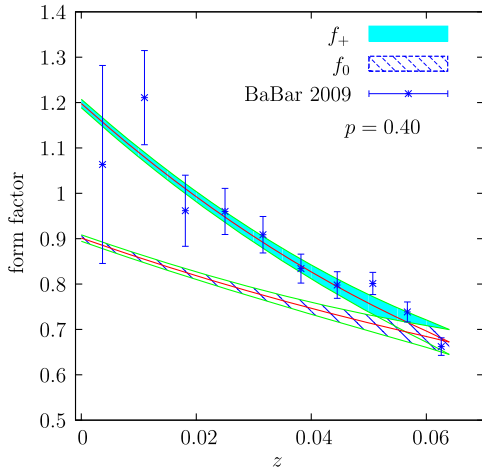
more correlated between w values. Given this consistency, we now proceed with the determination of $|V_{cb}|$ from a combined fit of the two data sets.

Table X shows the series coefficients and goodness of fit obtained for combined fits of the lattice and experimental data, imposing the kinematic constraint, for $N = 2$–4. Again, the fit, and in particular the error on $|V_{cb}|$, stabilizes by quadratic order. We choose $N = 3$ for our preferred fit, and plot the result in Fig. 11.

D. Comment on the CLN parametrization

The standard approach used by experimentalists to obtain $|V_{cb}|$ is to use the Caprini, Lellouch, Neubert

TABLE X.   Best-fit values of the z-expansion parameters for different truncations N from a joint fit to experimental data and lattice values. For completeness, the inferred value and error in $a_{0,0}$ is quoted. We also show the zero-recoil form factor $\mathcal{G}(1)$ and $|V_{cb}|$. Priors are imposed on coefficients of higher-order terms and degrees of freedom are counted as in Table VIII.

	$N = 2$	$N = 3$	$N = 4$
$a_{+,0}$	0.01260(10)	0.01261(10)	0.01261(10)
$a_{+,1}$	$-0.096(3)$	$-0.096(3)$	$-0.096(3)$
$a_{+,2}$	0.37(8)	0.37(11)	0.37(11)
$a_{+,3}$	$\cdots$	$-0.05(90)$	$-0.05(90)$
$a_{+,4}$	$\cdots$	$\cdots$	$-0.0(1.0)$
$a_{0,0}$	0.01140(9)	0.01140(9)	0.01140(9)
$a_{0,1}$	$-0.059(3)$	$-0.059(3)$	$-0.059(3)$
$a_{0,2}$	0.18(9)	0.19(10)	0.19(10)
$a_{0,3}$	$\cdots$	$-0.3(9)$	$-0.3(9)$
$a_{0,4}$	$\cdots$	$\cdots$	$-0.0(1.0)$
$\mathcal{G}(1)$	1.0527(82)	1.0528(82)	1.0528(82)
$|V_{cb}|$	0.0396(17)	0.0396(17)	0.0396(17)
χ^2/df	8.4/10	8.3/10	8.3/10

FIG. 11 (color online). Result of the preferred joint fit of the *BABAR* experimental data together with the lattice form factors. The plotted experimental points have been divided by our best-fit value of $\bar{\eta}_{\mathrm{EW}}|V_{cb}|$ and converted to f_+.

(CLN) parametrization [11] to extrapolate the experimental data to $w = 1$. Caprini, Lellouch, and Neubert use heavy-quark symmetry to derive more stringent constraints on the coefficients of the z-parametrization through $\mathcal{O}(z^3)$, resulting in a function with only two free parameters, $f_+(0)$ and ρ_1^2:

$$\frac{f_+(z)}{f_+(0)} = 1 - 8\rho_1^2 z + (51\rho_1^2 - 10)z^2 - (252\rho_1^2 - 84)z^3.$$

$$(5.6)$$

Use of the CLN parametrization in our analysis does not reduce the quoted errors in $|V_{cb}|$ despite the introduction of additional theoretical information.

The numerical values of the coefficients in Eq. (5.6) have theoretical uncertainties which can be estimated from the information given in tables and plots from Ref. [11]. To the best of our knowledge, however, CLN fits to experimental data do not incorporate the theoretical uncertainties discussed in Ref. [11], and may therefore be underestimating the uncertainty in $|V_{cb}|$. We have attempted to quantify the uncertainty from the use of the CLN form by incorporating the theoretical uncertainties in the CLN parameters via Bayesian priors. We did not find any difference in the error on $|V_{cb}|$ obtained from fits with and without including these theoretical uncertainties at the current level of precision. This is primarily because the $B \to D\ell\nu$ data displays little evidence of curvature in z within the present errors, and does not constrain the coefficient of the z^3 term. Nevertheless, we do not quote the results of our CLN fits in this work because we are more confident in the errors obtained from the model-independent z parametrization, Eq. (5.2), which can be used to obtain $|V_{cb}|$ even as the experimental and lattice uncertainties become arbitrarily more precise.

VI. DISCUSSION AND OUTLOOK

We obtain

$$|V_{cb}| = (39.6 \pm 1.7_{\mathrm{QCD+exp}} \pm 0.2_{\mathrm{QED}}) \times 10^{-3} \quad (6.1)$$

from our analysis of the exclusive decay $B \to Dl\nu$ at nonzero recoil, where the first error combines systematic and statistical errors from both experiment and theory and the second comes from the uncertainty in the correction for the final state Coulomb interaction in the B^0 decays. Because we provide the series coefficients of a z parametrization and their correlations, the result for $|V_{cb}|$ in Eq. (6.1) can be updated whenever new experimental information becomes available.

The combined error from lattice and experiment in $|V_{cb}|$ is about 4%. Because this error is obtained from a joint z-fit, the theory and experimental errors cannot be strictly disentangled, but they can be estimated as follows. In the right panel of Fig. 10 we plot the determinations of f_+ from separate z fits to the lattice form factors and to the experimental data. Inspection of the error bands shows that the combined error, which determines the uncertainty on $|V_{cb}|$, is smallest at about $z \approx 0.025$ ($w \approx 1.2$). At this point, the experimental error is about 3.9% and the lattice error is about 1.4%. (Note that combining them in quadrature yields a total that is close to the 4% lattice+experiment error on $|V_{cb}|$ from the joint fit.) Thus the experimental error currently limits the precision on $|V_{cb}|$ from this approach. The dominant uncertainty in the experimental data is the assumed 3.3% systematic error, which is used for all w values in the joint fit. Now that lattice-QCD results for the $B \to D\ell\nu$ form factors are available at nonzero recoil; however, it is clearly worthwhile to study and improve the systematic errors in the experimental data at medium and large recoil.

It is interesting to compare the above nonzero-recoil result with the result based on the standard method that uses only the zero-recoil extrapolation of the experimental and theoretical form factors. The z expansion fit to lattice-only data gives $\mathcal{G}(1) = 1.054(4)_{\mathrm{stat}}(8)_{\mathrm{syst}}$. The *BABAR* Collaboration quotes $\bar{\eta}_{\mathrm{EW}}|V_{cb}|\mathcal{G}(1) = 0.0430(19)_{\mathrm{stat}}(14)_{\mathrm{syst}}$ [9] from its B-tagged data, which gives $|V_{cb}| = (40.8 \pm 0.3_{\mathrm{QCD}} \pm 2.2_{\mathrm{exp}} \pm 0.2_{\mathrm{QED}}) \times 10^{-3}$. The result is consistent with the value from nonzero recoil, but the error is larger, as expected. Our zero-recoil form factor is consistent with a previous, preliminary Fermilab/MILC result of $\mathcal{G}(1) = 1.074(18)_{\mathrm{stat}}(16)_{\mathrm{syst}}$ [14], but with significantly smaller uncertainties due to the use of a much larger data set with several lattice spacings and lighter pions. We also note that the systematic error estimate for the earlier result did not include an estimate of the heavy-quark discretization errors, one of the larger contributions to the error in our new result.
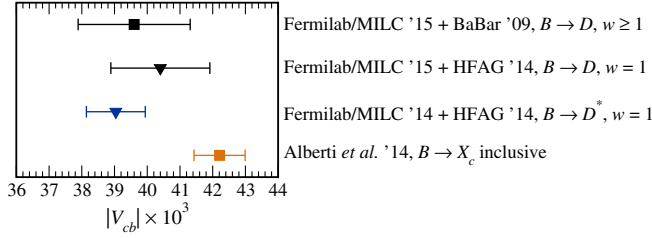
JON A. BAILEY *et al.*

PHYSICAL REVIEW D **92**, 034506 (2015)

FIG. 12 (color online). Comparison of exclusive and inclusive determinations of $|V_{cb}| \times 10^3$. Triangles denote an extrapolation to zero recoil, while squares use data over a wide kinematic range. The color code is black, blue (dark gray), and orange (light gray) for $B \to D\ell\nu$, $B \to D^*\ell\nu$, and $B \to X_c\ell\nu$, respectively.

We compare our result for $|V_{cb}|$ with other published determinations from inclusive and exclusive decays in Fig. 12. Our result is consistent with the determination from our companion analysis of $B \to D^*\ell\nu$ at zero recoil, $|V_{cb}| = (39.04 \pm 0.53_{\rm QCD} \pm 0.49_{\rm exp} \pm 0.19_{\rm QED}) \times 10^{-3}$ [5]. The errors on $|V_{cb}|$ from the current work are larger, however, because of the larger errors in the experimental data. Our result is 1.5σ lower than a recent inclusive (nonlattice) determination, $|V_{cb}| = (42.2 \pm 0.8_{\rm thy+exp}) \times 10^{-3}$ [7] which is also based on several experiments and employs data at nonzero recoil.

We also plot the result for $|V_{cb}|$ in Fig. 12 determined from only our zero-recoil lattice data, but using the best experimental knowledge of the extrapolated quantity $\bar{\eta}_{\rm EW}|V_{cb}|\mathcal{G}(1)$. The HFAG average value $\bar{\eta}_{\rm EW}|V_{cb}|\mathcal{G}(1)$ is $0.04264(72)_{\rm stat}(135)_{\rm syst}$ [3], which combines five experimental measurements from ALEPH [65], Belle [66], *BABAR* [9,67], and CLEO [68]. From this value we obtain $|V_{cb}| = (40.0 \pm 0.3_{\rm QCD} \pm 1.4_{\rm exp} \pm 0.2_{\rm QED}) \times 10^{-3}$. This error is smaller than that from the analysis at nonzero recoil, thanks to the additional experimental information, but only by about 10%. Thus combining lattice data at nonzero recoil with a single experiment reduces the error on $|V_{cb}|$ by almost as much as adding zero-recoil data from

several experiments. Clearly the error on $|V_{cb}|$ from $B \to D\ell\nu$ at nonzero recoil can be further reduced via a joint fit of the lattice form-factor data with additional experimental measurements once correlations are available.

An interesting byproduct of our combined z-expansion fit to obtain $|V_{cb}|$ is an improved determination of the $B \to D$ form factors $f_+(q^2)$ and $f_0(q^2)$. Because the lattice form factors are most accurate at high q^2, while the experimental measurements are most accurate at low q^2, they provide complimentary constraints on the form-factor shape. Table XI provides the z-fit coefficients and correlation matrix from our preferred combined lattice-experiment fit used to obtain our result for $|V_{cb}|$ quoted in Eq. (6.1). These represent our current best knowledge of $f_+(q^2)$ and $f_0(q^2)$ for $B \to D$ semileptonic decays, and can be used in other phenomenological applications. Here we use the results in Table XI to update our calculation of the ratio $\mathcal{B}(B \to D\tau\nu)/\mathcal{B}(B \to D\ell\nu)$ in the Standard Model [16]. We obtain

$$R(D) = 0.299(11), \qquad (6.2)$$

which agrees with our previous determination $R(D) = 0.316(12)(7)$ in [16], but is 2.0σ lower than the *BABAR* measurement $R(D) = 0.440(58)(42)$ [69]. The error in our new determination of $R(D)$ is about 20% smaller than in Ref. [16], primarily due to the inclusion of the experimental information on the shape of f_+ from the joint z-fit.

The dominant errors in the lattice form factors come from statistics, matching, and the chiral-continuum extrapolation, and can be reduced through simulations at smaller lattice spacings and at physical quark masses and from further study of the matching factors. The MILC Collaboration is currently generating $(2 + 1 + 1)$-flavor HISQ ensembles with physical light quarks [70], which we anticipate using for future calculations of $B \to D^{(*)}$ form factors. Heavy-quark discretization errors are also important. They can be reduced with a more improved

TABLE XI. Central values, errors, and correlation matrix for the parameters of the joint cubic fit to the synthetic lattice data for f_+ and f_0 (including the kinematic constraint at $q^2 = 0$) and the experimental measurements of $\bar{\eta}_{\rm EW}|V_{cb}|f_+(w)$. The coefficient $a_{0,0}$ was eliminated by the constraint, but we list it here for completeness. Its correlations with the other parameters are simply the coefficients of the linear constraint relation.

| | Value | Correlation matrix | | | | | | | |
		$a_{+,0}$	$a_{+,1}$	$a_{+,2}$	$a_{+,3}$	$a_{0,0}$	$a_{0,1}$	$a_{0,2}$	$a_{0,3}$
$a_{+,0}$	001261(10)	1.00000	0.24419	−0.08658	0.01207	1.05212	0.23370	0.03838	−0.05639
$a_{+,1}$	−00963(33)		1.00000	−0.57339	0.25749	0.06785	0.80558	−0.25493	−0.15014
$a_{+,2}$	037(11)			1.00000	−0.64492	0.00437	−0.44966	0.66213	0.05120
$a_{+,3}$	−005(90)				1.00000	0.00028	0.11311	−0.20100	0.23714
$a_{0,0}$	001142(14)					1.00000	−0.06448	−0.00416	−0.00027
$a_{0,1}$	−00590(28)						1.00000	−0.44352	0.02485
$a_{0,2}$	019(10)							1.00000	−0.46248
$a_{0,3}$	−003(87)								1.00000

034506-20

heavy-quark action such as that proposed in Ref. [71], and work on this is underway [72,73].

APPENDIX A: HEAVY-QUARK MASS CORRECTIONS

Heavy-quark masses (κ values) are determined by requiring that the kinetic masses of the D_s and B_s match their experimental values. The three-point and two-point functions in this study were computed with κ values from a preliminary tuning. Final tuned values differed slightly [5], as shown in Tables II and V.

We therefore need to adjust the form factors and w values accordingly. This is done by repeating the computation of the ratios R_+, $Q_+(\boldsymbol{p})$, and $\boldsymbol{R}_-(\boldsymbol{p})$ on the $a \approx 0.12$ fm, $\hat{m}' = 0.2m_s'$ ensemble for a few values of κ_b and κ_c in the vicinity of the desired, tuned values. These results permit calculating the derivatives of the form factors with respect to the quark masses. We assume that these results, expressed in dimensionless terms, can then be used to adjust form factors in our other ensembles.

From Eqs. (2.18)–(2.20), we see that we have the option of computing and applying these adjustments before or after matching with the ρ factors. Because of the simplifying steps taken in Appendix B for $\rho_{V^4}(w)/\rho_{V^4}(1)$ and $\rho_{V^i}(w)/\rho_{V^4}(w)$, we choose to make the adjustments directly on unmatched quantities. From Eqs. (2.22) and (2.23), one sees that it is convenient to study the mass dependence of

$$S_+ = \sqrt{R_+} Q_+, \tag{A1}$$

$$S_- = \frac{\boldsymbol{R}_- \cdot \boldsymbol{x}_f}{\boldsymbol{x}_f^2}, \tag{A2}$$

and $\boldsymbol{x}_f^2 S_-$.

Heavy-quark symmetry suggests that interpolations in inverse quark masses will implement the quark-mass tuning most smoothly. With the Fermilab method [17], the quark mass is identified with the kinetic mass:

$$\frac{1}{m_2 a} = \frac{2}{m_0 a(2 + m_0 a)} + \frac{1}{m_0 a + 1}, \tag{A3}$$

where we compute the bare quark mass $m_0 a$ from the tadpole-improved, tree-level formula

$$m_0 a = \frac{1}{u_0}\left(\frac{1}{2\kappa} - \frac{1}{2\kappa_{\mathrm{cr}}}\right). \tag{A4}$$

Here, u_0 is the tadpole parameter, and κ_{cr} is the value of κ such that the lightest pseudoscalar meson mass vanishes. Thus, below we compute slopes of S_+, S_-, and $\boldsymbol{x}_f^2 S_-$ with respect to $\xi_c = 1/(m_{2c}r_1)$ and $\xi_b = 1/(m_{2b}r_1)$. The results of the computations with varying quark masses are shown in Figs. 13 and 14.

Because the corrections in the charm and bottom masses are small, it suffices to work to first order in the inverse mass shift. Heavy-quark symmetry also suggests that the leading mass dependence of $S_+(w = 1) = \sqrt{R_+}$ is quadratic, of the form $(\xi_c - \xi_b)^2$. Therefore, the leading shift in ξ_c is suppressed by ξ_b, and the leading shift in ξ_b is suppressed by ξ_c. Below, we neglect the former effect but keep the latter, since it is suppressed only by ξ_c. Furthermore, by construction $\boldsymbol{x}_f^2 S_- \to 0$ as $w \to 1$ for all quark masses, and, therefore, the derivative with respect to
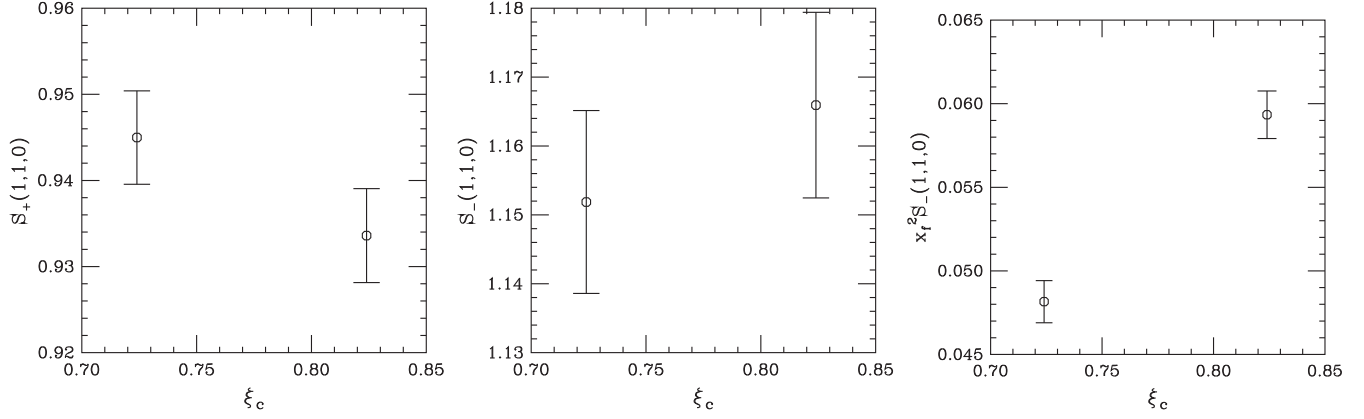
FIG. 13.   Heavy-quark mass dependence on the $a \approx 0.12$ fm, $\hat{m}' = 0.2m'_s$ ensemble at momentum $2\pi(1,1,0)/L$. Left to right: S_+, S_-, and $x_f^2 S_-$, respectively, vs inverse charm-quark kinetic mass $\xi_c = (m_{2c} r_1)^{-1}$.
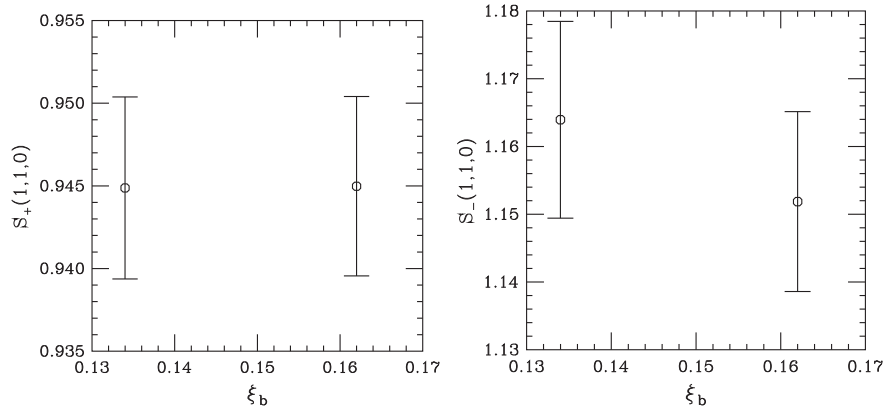

FIG. 14.   Heavy-quark mass dependence on the $a \approx 0.12$ fm, $\hat{m}' = 0.2m'_s$ ensemble at momentum $2\pi(1,1,0)/L$. S_+ (left) and S_- (right) vs inverse bottom-quark kinetic mass $\xi_b = (m_{2b} r_1)^{-1}$.

ξ_c also vanishes at $w = 1$. On the other hand, neither S_- nor its derivatives vanish at $w = 1$.

Because of the narrow range of w, $1 \leq w < 1.16$, for our data, one should expect a linear approximation in w to suffice for the quark-mass adjustments. Indeed, only $x_f^2 S_-$ requires a quadratic, as shown in Figs. 15 and 16. Therefore, we introduce

$$\frac{dS_+}{d\xi_c} = r_{+,1,c}(w - 1), \qquad (A5)$$

$$\frac{dS_-}{d\xi_c} = r_{-,0,c} + r_{-,1,c}(w - 1), \qquad (A6)$$

$$\frac{d(x_f^2 S_-)}{d\xi_c} = r_{x,1,c}(w - 1) + r_{x,2,c}(w - 1)^2, \qquad (A7)$$

$$\frac{dw}{d\xi_c} = r_{w,1,c}(w - 1), \qquad (A8)$$

$$\frac{dS_+}{d\xi_b} = r_{+,0,b} + r_{+,1,b}(w - 1), \qquad (A9)$$

$$\frac{dS_-}{d\xi_b} = r_{-,0,b} + r_{-,1,b}(w - 1). \qquad (A10)$$

(The notation for the slope parameters $r_{f,n,q}$ encodes a form factor label f, a polynomial coefficient index n, and a quark mass label q.) Fits to our data then yield

$$r_{+,1,c} = -0.72(5), \qquad (A11)$$

$$r_{-,0,c} = 0.102(11), \qquad (A12)$$

$$r_{-,1,c} = -0.23(14), \qquad (A13)$$

$$r_{x,1,c} = 0.851(14), \qquad (A14)$$

$$r_{x,2,c} = -1.22(16), \qquad (A15)$$

FIG. 15. Effect of heavy-quark mass shifts on the $a \approx 0.12$ fm, $\hat{m}' = 0.2m_s'$ ensemble as the charm-quark mass parameter is increased from $\kappa_c = 0.1254$ to 0.1280. Left to right: dS_+, dS_-, and $d(x_f^2 S_-)$, respectively, vs $w - 1$.
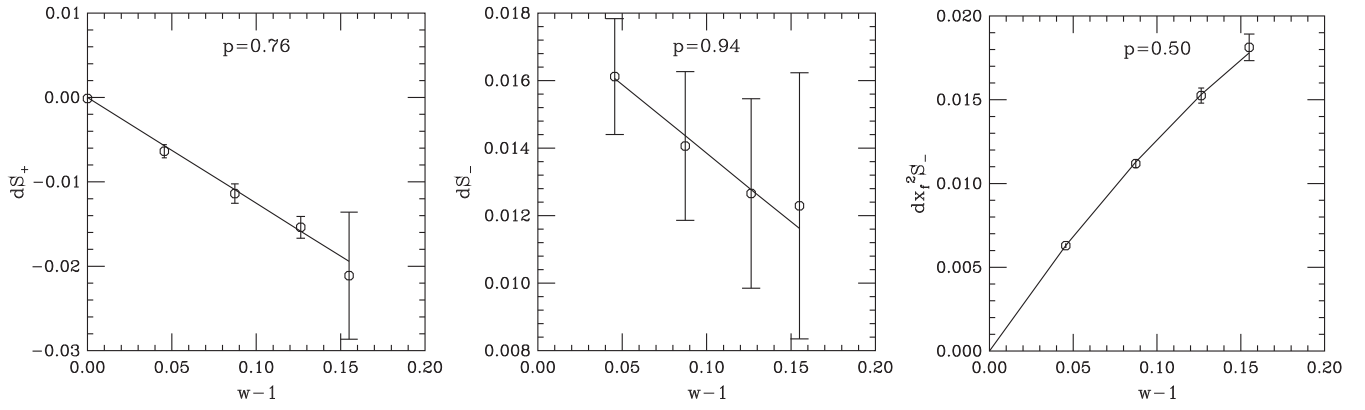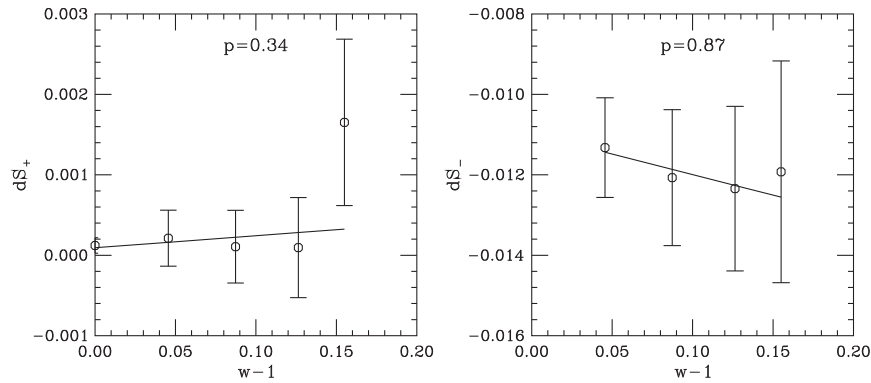

FIG. 16. Effect of heavy-quark mass shifts on the $a \approx 0.12$ fm, $\hat{m}' = 0.2m_s'$ ensemble as the bottom-quark mass parameter is increased from $\kappa_b = 0.0860$ to 0.0901 vs $w - 1$. Left to right: dS_+ and dS_-, respectively, vs $w - 1$.

$$r_{+,0,b} = 0.0042(41), \tag{A16}$$

$$r_{+,1,b} = 0.07(21), \tag{A17}$$

$$r_{-,0,b} = -0.49(5), \tag{A18}$$

$$r_{-,1,b} = -0.46(69). \tag{A19}$$

As discussed above, we expect $r_{+,0,b}$ to be of order ξ_c, or approximately 0.83. In fact, it is much smaller.

We compute the correlation functions at discrete values of the recoil momentum of the D meson, resulting in discrete values w_i, which are determined from Eqs. (2.15) and (2.17). The recoil variable w_i is determined dynamically from diagonal vector current matrix elements involving the D meson, so it varies with the charm quark mass, but not the bottom quark mass. We take the convention that when we shift both quark masses, we shift w_i to w_i' and we shift $S_+(w_i)$ to $S_+'(w_i')$, and similarly for S_- and $x_f^2 S_-$. As can be seen from Fig. 17, the data support a linear approximation for the shift in w_i also.

The effect of the kappa adjustment on the values of w, h_+, and h_- is illustrated in Table XII for the $a \approx 0.12$ fm, $\hat{m}' = 0.14m_s'$ ensemble where the tuning adjustment decreases both κ_c and κ_b from their simulation values.
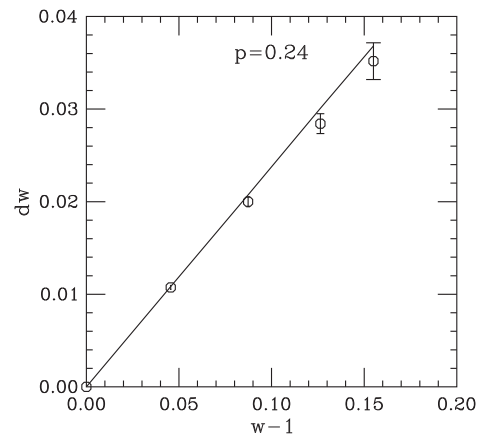

FIG. 17. Effect of heavy-quark mass shifts on the $a \approx 0.12$ fm, $\hat{m}' = 0.2m_s'$ ensemble. Shift in recoil variable w_i vs $w - 1$ as the charm-quark mass parameter is increased from $\kappa_c = 0.1254$ to 0.1280.

TABLE XII.   Unadjusted and adjusted values of w, h_+, and h_- for the $a \approx 0.12$ fm, $\hat{m}' = 0.14 m_s'$ ensemble. For this illustration only statistical errors are shown.

Momentum	Raw w	Shifted w	Raw h_+	Tuned h_+	Raw h_-	Tuned h_-
000	1	1	1.0391(53)	1.0390(53)	$\cdots$	$\cdots$
100	1.0465	1.0426	0.9812(61)	0.9849(62)	0.0041(111)	0.0008(111)
110	1.0896	1.0822	0.9388(70)	0.9457(70)	0.0072(134)	0.0031(135)
111	1.1299	1.1191	0.8978(97)	0.9073(97)	0.0139(165)	0.0092(166)
200	1.1553	1.1424	0.8789(120)	0.8898(121)	0.0336(205)	0.0286(206)

APPENDIX B: HEAVY-QUARK DISCRETIZATION EFFECTS

We use the heavy-quark effective theory (HQET) to derive the form of heavy-quark discretization effects [19,56]. In this appendix, we apply this formalism to derive the matching procedure from lattice gauge theory to continuum QCD; cf. Eqs. (2.18)–(2.20). We also use it to derive power-law discretization effects, both at nonzero recoil ($w > 1$) and at zero recoil ($w = 1$) where heavy-quark symmetry is more constraining. In the last subsection of the appendix, we also present numerical estimates for the discretization errors.

1. Formalism

We describe the underlying lattice gauge theory (LGT) with an effective Lagrangian, asserting the relation

$$\mathcal{L}_{\text{LGT}} \doteq \bar{h}(iv \cdot D - m_1)h + \frac{\bar{h}D_\perp^2 h}{2m_2} + \frac{\bar{h}s \cdot Bh}{2m_B}$$
$$+ \frac{\bar{h}[D_\perp^\alpha, iE_\alpha]h}{8m_D^2} + \frac{\bar{h}s_{\alpha\beta}\{D_\perp^\alpha, iE^\beta\}h}{4m_E^2} + \cdots, \quad (B1)$$

where $\doteq$ can be read "has the same matrix elements as." Here, v is a four vector specifying the rest frame of the heavy-light meson, such that $v^2 = -1$; the heavy-quark field h satisfies $\rlap{/}{v}h = ih$; and $s_{\alpha\beta} = -i\sigma_{\alpha\beta}/2$. Then, $D_\perp^\mu = D^\mu + v^\mu v \cdot D$ is the covariant derivative orthogonal to v, $B^{\alpha\beta} = (\delta_\mu^\alpha + v^\alpha v_\mu)F^{\mu\nu}(\delta_\nu^\beta + v^\beta v_\nu)$ is the chromomagnetic field (in the v frame), and $E^\beta = -v_\alpha F^{\alpha\beta}$ is the chromoelectric field (in the v frame). The HQET description for continuum QCD has the same structure

$$\mathcal{L}_{\text{QCD}} \doteq \bar{h}(iv \cdot D - m)h + \frac{\bar{h}D_\perp^2 h}{2m} + \frac{z_B\bar{h}s \cdot Bh}{2m}$$
$$+ \frac{z_D\bar{h}[D_\perp^\alpha, iE_\alpha]h}{8m^2} + \frac{z_E\bar{h}s_{\alpha\beta}\{D_\perp^\alpha, iE^\beta\}h}{4m^2} + \cdots.$$
$$(B2)$$

In this framework, matching and improvement boil down to choosing the parameters of the lattice Lagrangian, such that the Eq. (B1) reproduces Eq. (B2) term by term.

The rest mass m_1 does not influence matrix elements or mass splittings. In the Fermilab method, therefore, one tunes κ so that

$$\frac{1}{2m_2} = \frac{1}{2m}, \quad (B3)$$

and c_{SW} so that

$$\frac{1}{2m_B} = \frac{z_B}{2m} = \frac{1 + \mathcal{O}(\alpha_s)}{2m}, \quad (B4)$$

where the second equality follows because $z_B = 1 + \mathcal{O}(\alpha_s)$. In this work, we tune κ via the heavy-strange meson mass; for details of our procedures, see Appendix C of Ref. [5]. Furthermore, we choose c_{SW} at the tadpole-improved tree level, which makes the coefficient of the $\mathcal{O}(\alpha_s)$ error in Eq. (B4) small [74].

The Fermilab vector current, Eq. (2.8), has an HQET description too. Through dimension four [19]

$$V^\mu \doteq \bar{C}_{V_\parallel}^{\text{LGT}} v^\mu \bar{c}_{v'} b_v + \bar{C}_{V_\perp}^{\text{LGT}} \bar{c}_{v'} i\gamma_\perp^\mu b_v + \bar{C}_{V_{v'}}^{\text{LGT}} v_\perp'^\mu \bar{c}_{v'} b_v$$
$$- \sum_{a=1}^{14} \bar{B}_{Va}^{\text{LGT}} \bar{\mathcal{Q}}_{Va}^\mu + \cdots. \quad (B5)$$

The continuum-QCD current $\mathcal{V}^\mu$ can be described in the same way albeit with different $\bar{C}$ and $\bar{B}$ coefficients, denoted in this paper by omitting the label "LGT." Then $Z_{V^\mu} V^\mu \doteq \mathcal{V}^\mu$ if the Z factors are chosen to be [19]

$$Z_{V^4} \equiv \bar{Z}_{V_\parallel} = \bar{C}_{V_\parallel}/\bar{C}_{V_\parallel}^{\text{LGT}}, \quad (B6)$$

$$Z_{V^i} \equiv \bar{Z}_{V_\perp} = \bar{C}_{V_\perp}/\bar{C}_{V_\perp}^{\text{LGT}}. \quad (B7)$$

In practice, of course, such matching is only approximate. For example, the one-loop calculation of ρ_{V^4}, explained in Sec. III E, leads to a matching error of order α_s^2.

With the Fermilab currents most of the 14 dimension-four coefficients $\bar{B}_{Va}^{\text{LGT}}$ vanish at the tree level; the same holds for continuum QCD and the $\bar{B}_{Va}$. The exceptions multiply the operators

$$\bar{\mathcal{Q}}_{V1}^\mu = -v^\mu \bar{c}_{v'} \rlap{/}{D}_\perp b_v, \quad (B8)$$

$$\bar{Q}_{V2}^{\mu} = \bar{c}_{v'} i\gamma_{\perp}^{\mu} \overset{\leftrightarrow}{\mathcal{D}}_{\perp} b_{v}, \qquad (B9)$$

$$\bar{Q}_{V4}^{\mu} = -v'^{\mu} \bar{c}_{v'} \overset{\leftarrow}{\mathcal{D}}_{\perp'} b_{v}, \qquad (B10)$$

$$\bar{Q}_{V5}^{\mu} = \bar{c}_{v'} \overset{\rightarrow}{\mathcal{D}}_{\perp'} i\gamma_{\perp'}^{\mu} b_{v}. \qquad (B11)$$

At the tree level, their coefficients are

$$\bar{Z}_{V_{\parallel}} \bar{B}_{V1}^{\mathrm{LGT}} = \bar{Z}_{V_{\perp}} \bar{B}_{V2}^{\mathrm{LGT}} \equiv \frac{1}{2m_{3b}}, \qquad (B12)$$

$$\bar{Z}_{V_{\parallel}} \bar{B}_{V4}^{\mathrm{LGT}} = \bar{Z}_{V_{\perp}} \bar{B}_{V5}^{\mathrm{LGT}} \equiv \frac{1}{2m_{3c}}. \qquad (B13)$$

The improvement terms in the current, namely d_1, are chosen so that

$$\frac{1}{2m_3} = \frac{1}{2m_2} + \mathcal{O}(\alpha_s a), \qquad (B14)$$

for operators with label $a \in \{1, 2, 4, 5\}$. The other $\bar{B}_{Va}^{(\mathrm{LGT})}$ are of order α_s from the outset.

2. Matching factors

Equation (2.18) is well known from earlier work [19,20]. To establish Eqs. (2.19) and (2.20), let us start by defining $h_{\pm}^{\mathrm{LGT}}(w)$ for the lattice current V^{μ} in analogy with the decomposition in Eq. (2.4). These form factors $h_{\pm}^{\mathrm{LGT}}(w)$ are *not* the right-hand sides of Eqs. (2.22) and (2.23). The task here is to show how the ratios cancel some of the cutoff effects in $h_{\pm}^{\mathrm{LGT}}(w)$. Sometimes it is convenient to choose arbitrary v and v' when working out consequences of the HQET. The kinematics of our lattice-QCD correlators correspond to $v = (i, \mathbf{0})$ and $v' = (iw, \mathbf{v}')$.

The simplest case is the definition of the velocity via $D(\mathbf{0}) \to D(\mathbf{p})$ matrix elements:

$$\mathbf{x}_f(\mathbf{p}) = \mathbf{v}' \frac{h_+^{\mathrm{LGT}}(\mathbf{p}) - h_-^{\mathrm{LGT}}(\mathbf{p})}{(w+1)h_+^{\mathrm{LGT}}(\mathbf{p}) - (w-1)h_-^{\mathrm{LGT}}(\mathbf{p})} = \frac{\mathbf{v}'}{w+1}, \qquad (B15)$$

because $h_-^{\mathrm{LGT}} = 0$ for a flavor-conserving transition. This property follows from time-reversal invariance of the chosen current and arises independent of any matching considerations. The expression for w in Eq. (2.17) then follows immediately from $w^2 = 1 + \mathbf{v}'^2$ (when $\mathbf{v} = \mathbf{0}$).

Similarly, the other ratios are

$$Q_+(\mathbf{p}) = \frac{(w+1)h_+^{\mathrm{LGT}}(w) - (w-1)h_-^{\mathrm{LGT}}(w)}{2h_+^{\mathrm{LGT}}(1)}, \qquad (B16)$$

$$\mathbf{R}_-(\mathbf{p}) = \mathbf{v}' \frac{h_+^{\mathrm{LGT}}(w) - h_-^{\mathrm{LGT}}(w)}{(w+1)h_+^{\mathrm{LGT}}(w) - (w-1)h_-^{\mathrm{LGT}}(w)}, \qquad (B17)$$

with $w = w(\mathbf{p})$. These form factors, of course, are for the flavor-changing process.

Using the trace formalism explained in Ref. [56], it is straightforward to obtain the following expressions for $h_{\pm}^{\mathrm{LGT}}(w)$:

$$h_+^{\mathrm{LGT}}(w) = \bar{C}_+^{\mathrm{LGT}}(w)\Xi(w)$$
$$+ \frac{w-1}{2} \{\bar{B}_+^{\mathrm{LGT}}(w)[2\xi_3(w) - \bar{\Lambda}\xi(w)]$$
$$- \bar{B}_+^{\prime\mathrm{LGT}}(w)\bar{\Lambda}\xi(w)\}, \qquad (B18)$$

$$h_-^{\mathrm{LGT}}(w) = \frac{1}{2}(w+1)\bar{C}_-^{\mathrm{LGT}}(w)\Xi(w)$$
$$+ \bar{B}_-^{\mathrm{LGT}}(w)[2\xi_3(w) - \bar{\Lambda}\xi(w)]$$
$$- \bar{B}_-^{\prime\mathrm{LGT}}(w)\bar{\Lambda}\xi(w), \qquad (B19)$$

neglecting higher-dimension terms. The leading-dimension, short-distance coefficients are

$$\bar{C}_+^{\mathrm{LGT}}(w) = \bar{C}_{V_{\parallel}}^{\mathrm{LGT}}(w) + \frac{1}{2}(w-1)\bar{C}_-^{\mathrm{LGT}}(w), \qquad (B20)$$

$$\bar{C}_-^{\mathrm{LGT}}(w) = \bar{C}_{V_{\parallel}}^{\mathrm{LGT}}(w) - \bar{C}_{V_{\perp}}^{\mathrm{LGT}}(w) - (w+1)\bar{C}_{V_{v'}}^{\mathrm{LGT}}(w). \qquad (B21)$$

The $\bar{B}_{\pm}^{(\prime)\mathrm{LGT}}$ each contain several of the 14 $\bar{B}_{Va}^{\mathrm{LGT}}$ in Eq. (B5), and the detailed expressions are not illuminating. The Isgur-Wise function $\xi(w)$ and its generalizations $\xi_3(w)$ and

$$\Xi(w) = \xi(w) + \Sigma_2 A_1(w) + \Sigma_B[3A_3(w) + 2(w-1)A_2(w)] \qquad (B22)$$

parametrize the long-distance physics. In the context of lattice gauge theory, their discretization effects arise only from the light degrees of freedom. In Eq. (B22), $\xi(1) = 1$ and $A_1(1) = A_3(1) = 0$ by flavor conservation in HQET. In order to have compact formulas, the function Ξ contains some short-distance information, namely the mass combinations

$$\Sigma_X = \frac{1}{2m_{Xc}} + \frac{1}{2m_{Xb}}, \qquad X \in \{2, B, 3\}, \qquad (B23)$$

which depend on the short-distances a and m_Q^{-1}.

When using HQET to describe the heavy-quark limit of continuum QCD, the algebra is identical. The difference lies in the short-distance coefficients: in the notation used here, $\bar{C}_{V_{\parallel}}^{\mathrm{LGT}}$ etc. simply lose the superscript "LGT." Further, discretization effects of the light degrees of freedom disappear from the HQET quantities $\bar{\Lambda}$, $\xi(w)$, $\xi_3(w)$, and $A_i(w)$.

To derive the matching factors, we focus on the leading-dimension term. Then one finds

$$Q_+(\boldsymbol{p}) = \frac{w+1}{2} \frac{\bar{C}_{V_\parallel}^{\text{LGT}}(w)}{\bar{C}_{V_\parallel}^{\text{LGT}}(1)} \Xi(w), \qquad (\text{B24})$$

$$\boldsymbol{R}_-(\boldsymbol{p}) = \frac{\boldsymbol{v}'}{w+1} \frac{\bar{C}_{V_\perp}^{\text{LGT}}(w) + (w+1)\bar{C}_{v'}^{\text{LGT}}(w)}{\bar{C}_{V_\parallel}^{\text{LGT}}(w)}. \qquad (\text{B25})$$

Thus, to match these quantities to continuum QCD, one must multiply Q_+ and $\boldsymbol{R}_-$ by

$$\frac{\rho_{V^4}(w)}{\rho_{V^4}(1)} \equiv \frac{\rho_{V_\parallel}(w)}{\rho_{V_\parallel}(1)} = \frac{\bar{C}_{V_\parallel}(w)}{\bar{C}_{V_\parallel}^{\text{LGT}}(w)} \frac{\bar{C}_{V_\parallel}^{\text{LGT}}(1)}{\bar{C}_{V_\parallel}(1)}, \qquad (\text{B26})$$

$$\frac{\rho_{V^i}(w)}{\rho_{V^4}(w)} \equiv \frac{\rho_{V_{v'}}(w)}{\rho_{V_\parallel}(w)} = \frac{\bar{C}_{V_\perp}(w) + (w+1)\bar{C}_{v'}(w)}{\bar{C}_{V_\perp}^{\text{LGT}}(w) + (w+1)\bar{C}_{v'}^{\text{LGT}}(w)} \frac{\bar{C}_{V_\parallel}^{\text{LGT}}(w)}{\bar{C}_{V_\parallel}(w)}, \qquad (\text{B27})$$

respectively, to obtain $\mathcal{Q}_+$ and $\boldsymbol{R}_-$ in Eqs. (2.19) and (2.20).

One-loop calculations of the w dependence of these coefficients are not available, however. (The algebra with $\boldsymbol{p} \neq \boldsymbol{0}$ is much more voluminous.) We shall proceed with a further approximation for each of the two factors multiplying Q_+ and R_-. By construction in Eq. (B26),

$$\frac{\rho_{V_\parallel}(w)}{\rho_{V_\parallel}(1)} = 1 + \mathcal{O}(\alpha_s(w-1)). \qquad (\text{B28})$$

Because the w dependence arises only from the vertex diagram—the tadpoles on the legs cancel—the computed

coefficient should, like those in Table V, be small. Furthermore we note that $w - 1 < 0.16$ and that the w dependence disappears when $m_c a \to 0$. Hence we neglect this one-loop contribution and take $\rho_{V^4}(w)/\rho_{V^4}(1) = 1$. For the $\mathcal{O}(\alpha_s)$ error we use the following form:

$$\frac{\rho_{V^4}(w)}{\rho_{V^4}(1)} = 1 \pm \alpha_V(2/a)\rho_{V^4\text{max}}^{[1]}(w-1)m_{2c}a, \qquad (\text{B29})$$

where the values for $\alpha_V(2/a)$ are listed in Table V, and

$$\rho_{V^4\text{max}}^{[1]} = 0.1 \qquad (\text{B30})$$

is an upper bound on the size of the observed one-loop corrections to $\rho_{V^4}(1)$. In the mass region of interest, $\rho_{V^4}^{[1]} < \rho_{V^4\text{max}}^{[1]}$.

Equation (B29) gives an estimate of the error in the ratio $\rho_{V^4}(w)/\rho_{V^4}(1)$. The zero-recoil $\rho_{V^4}(1)$ is calculated at one-loop order in lattice perturbation theory and tabulated in Table V. We estimate the $\mathcal{O}(\alpha_s^2)$ truncation error, in the spirit of Ref. [5], by taking the coefficient as twice the largest first-order coefficient, $2\rho_{V^4\text{max}}^{[1]} = 0.2$. Hence, the error due to omitted higher order corrections is estimated as

$$\pm 2\rho_{V^4\text{max}}^{[1]}\alpha_V^2(2/a). \qquad (\text{B31})$$

The two errors are combined in quadrature to obtain the total systematic error in $\rho_{V^4}(w)$:

$$\pm \rho_{V^4}(1)\sqrt{[\rho_{V^4\text{max}}^{[1]}\alpha_V(2/a)(w-1)m_{2c}a]^2 + [2\rho_{V^4\text{max}}^{[1]}\alpha_V^2(2/a)/\rho_{V^4}(1)]^2}. \qquad (\text{B32})$$

For the factor in Eq. (B27) for R_-, note that most of our ensembles have $m_c a < 0.4$ and recall that as $m_c a \to 0$ with $m_b a$ fixed, the short-distance coefficients of the HQET with two heavy-quark fields tend to those with one heavy-quark field (for bottom) and a Dirac field (for charm). As shown in Ref. [19],

$$\lim_{m_c a \to 0} \bar{Z}_{V_\parallel}(w) = Z_{V_\parallel}, \qquad (\text{B33})$$

$$\lim_{m_c a \to 0} \bar{Z}_{V_\perp}(w) = Z_{V_\perp}, \qquad (\text{B34})$$

$$\lim_{m_c a \to 0} \bar{Z}_{V_\perp}(w)\bar{C}_{V_{v'}}^{\text{LGT}}(w) = \bar{C}_{V_{v'}}(w); \qquad (\text{B35})$$

the unbarred coefficients have no w dependence [44]. In practice, the error in these equations is of order $\alpha_s(a)m_c a$. We shall neglect this contribution and use

$$\frac{\rho_{V^i}(w)}{\rho_{V^4}(w)} \equiv \frac{\rho_{V_{v'}}(w)}{\rho_{V_\parallel}(w)} = \frac{Z_{V_\perp}}{Z_{V_\parallel}}. \qquad (\text{B36})$$

The one-loop calculation of the right-hand side can be done at zero recoil and is, thus, much simpler. The one-loop result is given in the right-most column of Table V. To account for the error due to the neglected $\mathcal{O}(\alpha_s m_c a)$ contribution, as in Eq. (B30) we consider the size of the one-loop coefficient for the range of b-quark masses used in this calculation, finding $\rho^{[1]} \leq 0.352$. With $\rho_{\text{max}}^{[1]} = 0.352$ we take the error as

$$\pm \alpha_V(2/a)\rho_{\text{max}}^{[1]}m_{2c}a. \qquad (\text{B37})$$

3. Discretization errors at nonzero recoil ($w > 1$)

Power-law discretization effects arise from the higher-dimension terms in Eqs. (B20) and (B21). The

discretization errors can be found by comparing the HQET description of lattice gauge theory to that of continuum QCD, as follows: substitute Eqs. (B18) and (B19) into Eqs. (B16) and (B17), multiply by the matching factors as in Eqs. (2.19) and (2.20), and form the combinations in Eqs. (2.22) and (2.23). The resulting HQET descriptions of the form factors are

$$
h_+(w) = \bar{C}_+(w)\Xi(w)
$$
$$
+ \frac{w-1}{2}\{\bar{B}_+^{\text{mis}}(w)[2\xi_3(w) + \bar{\Lambda}\xi(w)]
$$
$$
+ \bar{B}_-^{\prime\text{mis}}(w)\bar{\Lambda}\xi(w)\}, \tag{B38}
$$

$$
h_-(w) = \frac{1}{2}(w+1)\bar{C}_-(w)\Xi(w)
$$
$$
+ \bar{B}_-^{\text{mis}}(w)[2\xi_3(w) - \bar{\Lambda}\xi(w)] - \bar{B}_-^{\prime\text{mis}}(w)\bar{\Lambda}\xi(w), \tag{B39}
$$

where[4]

$$
\bar{B}_+^{(\prime)\text{mis}}(w) = \frac{\bar{B}_+^{(\prime)\text{LGT}}(w)}{\bar{C}_{V_\perp}^{\text{LGT}}(w) + (w+1)\bar{C}_{v'}^{\text{LGT}}(w)}
$$
$$
\times \left(\bar{C}_+(w) - \frac{w+1}{2}\frac{\bar{C}_-^{\text{LGT}}(w)\bar{C}_{V_\parallel}(w)}{\bar{C}_{V_\parallel}^{\text{LGT}}(w)}\right),
$$
$$
- \frac{\bar{B}_-^{(\prime)\text{LGT}}(w)}{\bar{C}_{V_\perp}^{\text{LGT}}(w) + (w+1)\bar{C}_{v'}^{\text{LGT}}(w)}
$$
$$
\times \left(\bar{C}_-(w) - \frac{\bar{C}_-^{\text{LGT}}(w)\bar{C}_{V_\parallel}(w)}{\bar{C}_{V_\parallel}^{\text{LGT}}(w)}\right), \tag{B40}
$$

$$
\bar{B}_-^{(\prime)\text{mis}}(w) = \frac{\bar{B}_-^{(\prime)\text{LGT}}(w)}{\bar{C}_{V_\perp}^{\text{LGT}}(w) + (w+1)\bar{C}_{v'}^{\text{LGT}}(w)}
$$
$$
\times \left(\bar{C}_+(w) - w\bar{C}_-(w) + \frac{w-1}{2}\frac{\bar{C}_-^{\text{LGT}}(w)\bar{C}_{V_\parallel}(w)}{\bar{C}_{V_\parallel}^{\text{LGT}}(w)}\right),
$$
$$
- \frac{w^2-1}{4}\frac{\bar{B}_+^{(\prime)\text{LGT}}(w)}{\bar{C}_{V_\perp}^{\text{LGT}}(w) + (w+1)\bar{C}_{v'}^{\text{LGT}}(w)}
$$
$$
\times \left(\bar{C}_-(w) - \frac{\bar{C}_-^{\text{LGT}}(w)\bar{C}_{V_\parallel}(w)}{\bar{C}_{V_\parallel}^{\text{LGT}}(w)}\right). \tag{B41}
$$

As long as the matching of the dimension-three currents is carried out to order α_s^ℓ, the parts of Eqs. (B40) and (B41) entailing the $\bar{C}$ coefficients collapses such that

---

[4]The continuum QCD analogs of Eqs. (B40) and (B41) can be obtained by erasing the superscript "LGT" and simplifying with Eqs. (B20) and (B21). The result becomes, as expected, trivial.

$$
\bar{B}_\pm^{(\prime)\text{mis}} = \bar{B}_\pm^{(\prime)} + \mathcal{O}(\alpha_s^{\min(k,\ell)+1}), \tag{B42}
$$

where the dimension-four currents have been matched through order α_s^k. In particular at the tree level ($k=0$),

$$
\bar{B}_\pm^{\text{mis}} = \frac{1}{2m_{c3}} \pm \frac{1}{2m_{b3}}, \tag{B43}
$$

$$
\bar{B}_\pm^{\prime\text{mis}} = 0, \tag{B44}
$$

while in continuum QCD, $\bar{B}_\pm = 1/2m_c \pm 1/2m_b$ and $\bar{B}_\pm' = 0$. Thus, we have tree-level matching in the dimension-four currents, with errors from this source of the form

$$
\text{error}_{3,\pm} = [f_3(m_{0c}a) \pm f_3(m_{0b}a)]\bar{\Lambda}a. \tag{B45}
$$

Here $af_3(m_0a) = 1/2m_3 - 1/2m_2$, and the factor of $\bar{\Lambda}$ is a power-counting estimate of the HQET matrix element; $\bar{\Lambda}$ is the scale of nonperturbative QCD as it pertains to heavy-light mesons, roughly the difference between the heavy-light-meson and heavy-quark masses.

Another discretization error arises from the function $\Xi(w)$ in lattice gauge theory and continuum QCD. In LGT, the kinetic and chromomagnetic masses appear. In this way, one finds that the mismatch in Σ_B in $\Xi(w)$ yields an error

$$
\text{error}_B = [f_B(m_{0c}a) + f_B(m_{0b}a)](w-1)\bar{\Lambda}a, \tag{B46}
$$

taking the functions A_i to be of order $\bar{\Lambda}$ and building in the fact that the contribution vanishes as $w \to 1$. Similarly to the above, $af_B(m_0a) = 1/2m_B - 1/2m_2$, which, for our choice of c_{SW}, is of order α_s.

Combining the two kinds of errors ($\oplus$ means to add in quadrature),

$$
h_+(2.22) - h_+(\text{cont}) = \text{error}_B \oplus \frac{1}{2}(w-1)\text{error}_{3,+}, \tag{B47}
$$

$$
h_-(2.23) - h_-(\text{cont}) = \text{error}_{3,-}. \tag{B48}
$$

Because $\bar{C}_-$ vanishes at the tree level, the contribution to the error in h_- from $\bar{C}_-\text{error}_B$ is suppressed by an addition factor of α_s and, thus, omitted here. Note that $\text{error}_{3,+}$ in $h_+(w)$ is multiplied by $(w-1)$, whereas $\text{error}_{3,-}$ in $h_-(w)$ is not; cf. Eqs. (B38) and (B39). Our choices for the functions $f_B(m_0a)$ and $f_3(m_0a)$ are discussed below; cf. Eqs. (B58) and (B59).

4. Discretization errors at zero recoil ($w = 1$)

Because the next-to-leading-dimension discretization effects are suppressed by α_s, the next-to-next-to-leading-dimension effects may be of the same size. This is especially true at zero recoil, where the next-to-leading

contributions to h_+ vanish. To capture the leading discretization errors of $h_+(1)$, therefore, one needs the dimension-five temporal vector current (with $v' = v$) [56]:

$$
\begin{aligned}
Z_{V_{cb}^4} V^4 &= -Z_{V_{cb}^4} v \cdot V \\
&\doteq \bar{C}_{V_{\parallel}^{cb}} \bar{c}_v b_v + z_{V^{cb}1}^{(1,1)} \frac{\bar{c}_v \overleftarrow{D}_\perp \cdot D_\perp b_v}{2m_{3c} 2m_{3b}} \\
&+ z_{V^{cb}s}^{(1,1)} \frac{\bar{c}_v \overleftarrow{D}_\perp^\alpha s_{\alpha\beta} D_\perp^\beta b_v}{2m_{3c} 2m_{3b}} + \eta_{V^{cb}D_\perp^2}^{(0,2)} \frac{\bar{c}_v D_\perp^2 b_v}{8m_{D_\perp^2 b}^2} \\
&+ \eta_{V^{cb}sB}^{(0,2)} \frac{\bar{c}_v s \cdot B b_v}{8m_{sBb}^2} + \eta_{V^{cb}\alpha E}^{(0,2)} \frac{\bar{c}_v i\not{E} b_v}{4m_{\alpha Eb}^2} \\
&+ \eta_{V^{cb}D_\perp^2}^{(2,0)} \frac{\bar{c}_v \overleftarrow{D}_\perp^2 b_v}{8m_{D_\perp^2 c}^2} + \eta_{V^{cb}sB}^{(2,0)} \frac{\bar{c}_v s \cdot B b_v}{8m_{sBc}^2} \\
&+ \eta_{V^{cb}\alpha E}^{(2,0)} \frac{\bar{c}_v i\not{E} b_v}{4m_{\alpha Ec}^2},
\end{aligned}
\tag{B49}
$$

and similarly for $-v \cdot \mathcal{V}$. For the currents defined in Sec. II, as well as for the continuum currents, the η-coefficients and z-coefficients in Eq. (B49) all take the form $1 + \mathcal{O}(\alpha_s)$. The η-like coefficients and associated masses in Eq. (B49) drop out of the analysis.

From Eqs. (7.23)–(7.29) of Ref. [56], the HQET expansions through $\mathcal{O}(\bar{\Lambda}^2)$ of the matrix elements are

$$
\sqrt{\mathcal{R}_+} = \eta_V W_{00}^{(0)} + \bar{W}_{00}^{(2)},
\tag{B50}
$$

where η_V is an HQET-to-QCD matching factor that starts with 1 in perturbative QCD, and

$$
W_{00}^{(0)} = 1 - \frac{1}{2}\Delta_2^2 D - 3\Delta_2\Delta_B E - \frac{1}{2}\Delta_B^2(R_1 + 3R_2), \quad \text{(B51)}
$$

$$
\bar{W}_{00}^{(2)} = -\frac{1}{2}\Delta_3^2 [z_{V1}^{(1,1)}\mu_\pi^2 - z_{Vs}^{(1,1)}\mu_G^2],
\tag{B52}
$$

where D, E, R_1, R_2, μ_π^2, and μ_G^2 are HQET matrix elements of order $\bar{\Lambda}^2$.[5] Also,

$$
\Delta_I = \frac{1}{2m_{Ic}} - \frac{1}{2m_{Ib}}, \qquad I = 2, B, 3
\tag{B53}
$$

are combinations of the mass coefficients in Eqs. (B1) and (B14). Beyond the leading 1, the terms in $W_{00}^{(0)}$ come from double insertions of the kinetic and chromomagnetic interactions. $\bar{W}_{00}^{(2)}$ stems from the dimension-five currents in Eq. (B49).

Taking the difference between these expressions and the analogous ones for continuum QCD, one sees that the error in $W_{00}^{(0)}$ stems from

$$
\frac{1}{2m_{Bh}} - \frac{z_B}{2m_{2h}} = af_B(m_{0h}a).
\tag{B54}
$$

The coefficients $z_{J\bullet}^{(1,1)} = 1 + \mathcal{O}(\alpha_s)$; also $1/m_{3h} \to 1/m_h + \mathcal{O}(\alpha_s a)$ [compare Eqs. (B12) and (B13)]. Thus, the error entering $\bar{W}_{00}^{(2)}$ stems from

$$
\Delta_3^2 z_{V\bullet}^{(1,1)} - \Delta_2^2 z_{V\bullet}^{(1,1)} = 2a[f_3(m_{0c}a) - f_3(m_{0b}a)]\Delta_2,
\tag{B55}
$$

with f_3 of order α_s for our choices. Thus, errors in $\rho_{V^4}\sqrt{R_+}$ stem from the mismatches

$$
\begin{aligned}
&W_{00}^{(0)}(\text{LGT}) - W_{00}^{(0)}(\text{cont}) \\
&\quad = -a\Delta_2[f_B(m_{0c}a) - f_B(m_{0b}a)](R_1 + 3R_2 + 3E),
\end{aligned}
\tag{B56}
$$

$$
\begin{aligned}
&\bar{W}_{00}^{(2)}(\text{LGT}) - \bar{W}_{00}^{(2)}(\text{cont}) \\
&\quad = -a\Delta_2[f_3(m_{0c}a) - f_3(m_{0b}a)](\mu_\pi^2 - \mu_G^2).
\end{aligned}
\tag{B57}
$$

In estimating heavy-quark discretization errors, we use these results at $w = 1$, where the more generic effects in Eqs. (B47) and (B48) are much smaller.

5. Numerical estimates

For the mismatch functions f_B and f_3 in Eqs. (B46) and (B45), and in Eqs. (B56) and (B57), we use the functional forms [40]

$$
f_B(m_0 a) = \frac{\alpha_s}{2(1 + m_0 a)},
\tag{B58}
$$

$$
f_3(m_0 a) = \frac{\alpha_s}{2(2 + m_0 a)}.
\tag{B59}
$$

To estimate the HQET matrix elements, we take $\bar{\Lambda} = 450$ MeV,[6]

$$
\mu_G^2 = \frac{3}{4}(M_{B^*}^2 - M_B^2) = 0.364 \text{ GeV}^2 = (603 \text{ MeV})^2,
\tag{B60}
$$

$$
\mu_\pi^2(1 \text{ GeV}) = 0.424 \pm 0.042 \text{ GeV}^2 = (651 \pm 32 \text{ MeV})^2.
\tag{B61}
$$

---

[5]Reference. [56] used a notation setting $\mu_\pi^2 = -\lambda_1$ and $\mu_G^2 = 3\lambda_2$.

[6]Here, 450 MeV is not an estimate of $M_B - m_b$, but simply a practical number for power-counting estimates.

TABLE XIII. Absolute difference of $h_{\pm}(w)$ from mismatches in the heavy-quark Lagrangian and current. We take $\bar{\Lambda} = 450$ MeV, $\mu_\pi^2 = 0.424$ GeV^2, and $\mu_G^2 = 0.364$ GeV^2. We further estimate the quantity $|R_1 + 3R_2 + 3E|$ with $\bar{\Lambda}^2$. The totals are obtained from Eqs. (B47), (B48), and (B56) and (B57) for $h_+(w)$, h_-, and $h_+(1)$, respectively. The column for $h_+(w)$ must be multiplied by $(w-1)$. The difference is estimated using the $a = 0.09$ fm lattice as a baseline.

a (fm)	$\alpha_V(q^*)$	$m_{0b}a$	$m_{0c}a$	$h_+(w)$	$h_-(w)$, $\forall$ w	$h_+(1)$
0.120	0.300	2.462	0.532	−0.0095	−0.0030	−0.0011
0.090	0.261	1.664	0.362	0.0000	0.0000	0.0000
0.060	0.220	1.123	0.240	0.0109	0.0021	0.0011
0.045	0.198	0.808	0.176	0.0160	0.0029	0.0016

TABLE XIV. Absolute error on $h_{\pm}(w)$ from mismatches in the heavy-quark Lagrangian and current. We take $\bar{\Lambda} = 450$ MeV, $\mu_\pi^2 = 0.424$ GeV^2, and $\mu_G^2 = 0.364$ GeV^2. We further estimate the quantity $|R_1 + 3R_2 + 3E|$ with $\bar{\Lambda}^2$. The columns for $h_+(w)$ correspond to the chromomagnetic mismatch ["B," Eq. (B46)], the current mismatch ["3," Eq. (B45)], and their quadrature sum ["$\oplus$," Eq. (B47)]; these columns must be multiplied by $(w-1)$. The column for $h_-(w)$ comes from the mismatch in Eq. (B48). The columns for $h_+(1)$ correspond to the second-order mismatch of the Lagrangian ["$W_{00}^{(0)}$," Eq. (B56)] and the second-order mismatch of the current ["$\bar{W}_{00}^{(2)}$," Eq. (B57)], and their quadrature sum ("$\oplus$").

a (fm)	$\alpha_V(q^*)$	$m_{0b}a$	$m_{0c}a$	$h_+(w)$			$h_-(w)$	$h_+(1)$		
				B	3	$\oplus$	$\forall w$	$W_{00}^{(0)}$	$\bar{W}_{00}^{(2)}$	$\oplus$
0.120	0.300	2.462	0.532	0.0382	0.0125	0.0402	0.0069	0.0033	0.0005	0.0033
0.090	0.261	1.664	0.362	0.0293	0.0092	0.0307	0.0040	0.0023	0.0003	0.0023
0.060	0.220	1.123	0.240	0.0190	0.0057	0.0198	0.0019	0.0012	0.0001	0.0012
0.045	0.198	0.808	0.176	0.0141	0.0041	0.0147	0.0010	0.0007	0.0001	0.0007

We do not have estimates for D, E, R_1, and R_2 as good as Eqs. (B60) and (B61), but in Ref. [5] we found that we could explain the discretization effects at zero recoil in $B \to D^*$ with $|R_1 + 3R_2 + 3E| \lesssim (450 \text{ MeV})^2$.

We take the typical $\alpha_V(q^*)$ to be 0.262 on the $a \approx 0.09$ fm lattices, and we use one-loop running to obtain $\alpha_V(q^*)$ at the other lattice spacings.

In Table XIII, we show results from using these inputs to compute the differences that Eqs. (B56) and (B57) predict, using the lattice with $a \approx 0.09$ fm as the baseline. The estimates of the differences are compatible with the lattice-spacing dependence that can been seen for $w = 1$ in Fig. 7, and can be inferred for $w > 1$ from Fig. 3. For example, the error in $h_+(w)$ grows slowly with w, both from Table XIII [adding in quadrature the right-most column with $(w-1)$ times the fifth column] and Fig. 3. Because the *differences* from lattice to lattice are well described by the theory, we can proceed to use the same ideas to estimate the difference from each lattice to the continuum. The results of these calculations are shown in Table XIV. For our final error estimates on the vector and scalar form factors, we take the absolute errors on h_+ and h_- in Table XIV at $a \approx 0.06$ fm, and combine them in quadrature following Eqs. (2.5) and (2.6) that relate f_+ and f_0 to h_+ and h_-. The resulting expressions for the absolute errors as a function of recoil are

$$\text{error}_+ = \left[0.0198(w-1)\frac{1+r}{2\sqrt{r}} \right] \oplus \left[0.0019\frac{1-r}{2\sqrt{r}} \right]$$
$$\oplus \, 0.0012\frac{1+r}{2\sqrt{r}}, \tag{B62}$$

$$\text{error}_0 = \left[0.0198(w^2-1)\frac{\sqrt{r}}{1+r} \right] \oplus \left[0.0019(w-1)\frac{\sqrt{r}}{1-r} \right]$$
$$\oplus \, 0.0012(w+1)\frac{\sqrt{r}}{1+r}. \tag{B63}$$

These lead to estimates that range from 0.1%–0.4% for both f_+ and f_0 in our range of simulated lattice w values.

[1] A. X. El-Khadra, *Proc. Sci.*, LATTICE2013 (2014) 001 [arXiv:1403.5252].

[2] J. Charles, S. Descotes-Genon, Z. Ligeti, S. Monteil, M. Papucci, and K. Trabelsi, Phys. Rev. D **89,** 033016 (2014).

[3] Y. Amhis *et al.* (Heavy Flavor Averaging Group), (2012).

[4] S.-W. Qiu *et al.* (Fermilab Lattice and MILC Collaborations), *Proc. Sci.*, LATTICE2013 (2013) 385 [arXiv: 1312.0155].

[5] J. A. Bailey *et al.* (Fermilab Lattice and MILC Collaborations), Phys. Rev. D **89,** 114504 (2014).

[6] P. Gambino and C. Schwanda, Phys. Rev. D **89,** 014022 (2014).

[7] A. Alberti, P. Gambino, K. J. Healey, and S. Nandi, Phys. Rev. Lett. **114,** 061802 (2015).

[8] A. Crivellin and S. Pokorski, Phys. Rev. Lett. **114,** 011802 (2015).

[9] B. Aubert *et al.* (*BABAR* Collaboration), Phys. Rev. Lett. **104,** 011802 (2010).

[10] R. Glattauer (Belle Collaboration), in *Proceedings of ICHEP 2014*, http://indico.ific.uv.es/indico/getFile.py/ access?contribId=405&sessionId=25&resId=0&materialId= slides&confId=2025.

[11] I. Caprini, L. Lellouch, and M. Neubert, Nucl. Phys. **B530,** 153 (1998).

[12] C. G. Boyd, B. Grinstein, and R. F. Lebed, Phys. Rev. Lett. **74,** 4603 (1995).

[13] G. de Divitiis, E. Molinaro, R. Petronzio, and N. Tantalo, Phys. Lett. B **655,** 45 (2007).

[14] M. Okamoto *et al.* (Fermilab Lattice and MILC Collaborations), Nucl. Phys. B, Proc. Suppl. **140,** 461 (2005).

[15] J. A. Bailey *et al.* (Fermilab Lattice and MILC Collaborations), Phys. Rev. D **85,** 114502 (2012).

[16] J. A. Bailey *et al.*, Phys. Rev. Lett. **109,** 071802 (2012).

[17] A. X. El-Khadra, A. S. Kronfeld, and P. B. Mackenzie, Phys. Rev. D **55,** 3933 (1997).

[18] A. X. El-Khadra, A. S. Kronfeld, P. B. Mackenzie, S. M. Ryan, and J. N. Simone, Phys. Rev. D **64,** 014502 (2001).

[19] J. Harada, S. Hashimoto, A. S. Kronfeld, and T. Onogi, Phys. Rev. D **65,** 094514 (2002).

[20] S. Hashimoto, A. S. Kronfeld, P. B. Mackenzie, S. M. Ryan, and J. N. Simone, Phys. Rev. D **66,** 014503 (2002).

[21] C. W. Bernard, T. Burch, K. Orginos, D. Toussaint, T. A. DeGrand, C. DeTar, S. Datta, S. Gottlieb, Urs M. Heller, and R. Sugar, Phys. Rev. D **64,** 054506 (2001).

[22] C. Aubin, C. Bernard, C. DeTar, J. Osborn, S. Gottlieb, E. B. Gregory, D. Toussaint, U. M. Heller, J. E. Hetrick, and R. Sugar, Phys. Rev. D **70,** 094505 (2004).

[23] A. Bazavov *et al.*, Rev. Mod. Phys. **82,** 1349 (2010).

[24] M. Wingate, J. Shigemitsu, C. T. H. Davies, G. P. Lepage, and H. D. Trottier, Phys. Rev. D **67,** 054505 (2003).

[25] C. A. Aubin *et al.* (MILC Collaboration), Lattice QCD gauge ensemble: USQCD/MILC/asqtad/2064f21b679m020m050, doi:10.15484/milc.asqtad.en09a/1178163 (2015); Lattice QCD gauge ensemble: USQCD/MILC/asqtad/ 2064f21b679m020m050b, doi:10.15484/milc.asqtad.en09b/ 1178164 (2015).

[26] C. A. Aubin *et al.* (MILC Collaboration), Lattice QCD gauge ensemble: USQCD/MILC/asqtad/2064f21b676m010m050, doi:10.15484/milc.asqtad.en06a/1178158 (2015);

[27] Lattice QCD gauge ensemble: USQCD/MILC/asqtad/ 2064f21b676m010m050b, doi:10.15484/milc.asqtad.en06b/ 1178159 (2015).

[27] C. A. Aubin *et al.* (MILC Collaboration), Lattice QCD gauge ensemble: USQCD/MILC/asqtad/2064f21b676m007m050, doi:10.15484/milc.asqtad.en05a/1178156 (2015); Lattice QCD gauge ensemble: USQCD/MILC/asqtad/ 2064f21b676m007m050b, doi:10.15484/milc.asqtad.en05b/ 1178157 (2015).

[28] C. A. Aubin *et al.* (MILC Collaboration), Lattice QCD gauge ensemble: USQCD/MILC/asqtad/2464f21b676m005m050, doi:10.15484/milc.asqtad.en04a/1178155 (2015).

[29] C. A. Aubin *et al.* (MILC Collaboration), Lattice QCD gauge ensemble: USQCD/MILC/asqtad/2896f21b711m0124m031, doi:10.15484/milc.asqtad.en17a/1178099 (2015).

[30] C. A. Aubin *et al.* (MILC Collaboration), Lattice QCD gauge ensemble: USQCD/MILC/asqtad/2896f21b709m0062m031, doi:10.15484/milc.asqtad.en15a/1178095 (2015); Lattice QCD gauge ensemble: USQCD/MILC/asqtad/ 2896f21b709m0062m031b, doi:10.15484/milc.asqtad.en15b/ 1178096 (2015); Lattice QCD gauge ensemble: USQCD/ MILC/asqtad/2896f21b709m0062m031c, doi:10.15484/mil- c.asqtad.en15c/1178097 (2015).

[31] C. A. Aubin *et al.* (MILC Collaboration), Lattice QCD gauge ensemble: USQCD/MILC/asqtad/3296f21b7085m00465m031, doi:10.15484/milc.asqtad.en14a/1178094 (2015).

[32] C. A. Aubin *et al.* (MILC Collaboration), Lattice QCD gauge ensemble: USQCD/MILC/asqtad/4096f21b708m0031m031a, doi:10.15484/milc.asqtad.en13a/1178092 (2015); Lattice QCD gauge ensemble: USQCD/MILC/asqtad/ 4096f21b708m0031m031b, doi:10.15484/milc.asqtad.en13b/ 1178093 (2015).

[33] C. A. Aubin *et al.* (MILC Collaboration), Lattice QCD gauge ensemble: USQCD/MILC/asqtad/6496f21b7075m00155m031, doi:10.15484/milc.asqtad.en12a/1178091 (2015).

[34] C. A. Aubin *et al.* (MILC Collaboration), Lattice QCD gauge ensemble: USQCD/MILC/asqtad/48144f21b748m0072m018a, doi:10.15484/milc.asqtad.en23a/1178040 (2015); Lattice QCD gauge ensemble: USQCD/MILC/asqtad/ 48144f21b748m0072m018b, doi:10.15484/milc.asqtad.en23b/ 1178041 (2015).

[35] C. A. Aubin *et al.* (MILC Collaboration), Lattice QCD gauge ensemble: USQCD/MILC/asqtad/48144f21b747m0036m018a, doi:10.15484/milc.asqtad.en20a/1178036 (2015); Lattice QCD gauge ensemble: USQCD/MILC/asqtad/ 48144f21b747m0036m018b, doi:10.15484/milc.asqtad.en20b/ 1178037 (2015).

[36] C. A. Aubin *et al.* (MILC Collaboration)Lattice QCD gauge ensemble: USQCD/MILC/asqtad/56144f21b7465m0025m018, doi:10.15484/milc.asqtad.en19a/1178035 (2015).

[37] C. A. Aubin *et al.* (MILC Collaboration), Lattice QCD gauge ensemble: USQCD/MILC/asqtad/64144f21b746m0018m018a, doi:10.15484/milc.asqtad.en18a/1178033 (2015); Lattice QCD gauge ensemble: USQCD/MILC/asqtad/ 64144f21b746m0018m018b, doi:10.15484/milc.asqtad.en18b/ 1178034 (2015).

[38] C. A. Aubin *et al.* (MILC Collaboration), Lattice QCD gauge ensemble: USQCD/MILC/asqtad/64192f21b781m0028m014, doi:10.15484/milc.asqtad.en24a/1177873 (2015).

[39] D. P. Menscher, Ph.D. thesis, University of Illinois, 2005.

[40] A. Bazavov *et al.* (Fermilab Lattice and MILC Collaborations), Phys. Rev. D **85**, 114506 (2012).

[41] C. Bernard *et al.* (Fermilab Lattice and MILC Collaborations), Phys. Rev. D **79**, 014506 (2009).

[42] J. A. Bailey *et al.* (Fermilab Lattice and MILC Collaborations), Phys. Rev. D **79**, 054507 (2009).

[43] G. P. Lepage and P. B. Mackenzie, Phys. Rev. D **48**, 2250 (1993).

[44] J. Harada, S. Hashimoto, K.-I. Ishikawa, A. S. Kronfeld, T. Onogi, and N. Yamada, Phys. Rev. D **65**, 094513 (2002).

[45] C.-K. Chow and M. B. Wise, Phys. Rev. D **48**, 5202 (1993).

[46] J. Laiho and R. S. Van de Water, Phys. Rev. D **73**, 054501 (2006).

[47] A. Anastassov *et al.* (CLEO Collaboration), Phys. Rev. D **65**, 032003 (2002).

[48] J. Lees *et al.* (*BABAR* Collaboration), Phys. Rev. D **88**, 052003 (2013).

[49] J. Lees *et al.* (*BABAR* Collaboration), Phys. Rev. Lett. **111**, 111801 (2013).

[50] W. Detmold, C.-J. D. Lin, and S. Meinel, Phys. Rev. Lett. **108**, 172003 (2012).

[51] K. U. Can, G. Erkol, M. Oka, A. Ozpineci, and T. T. Takahashi, Phys. Lett. B **719**, 103 (2013).

[52] D. Becirevic and F. Sanfilippo, Phys. Lett. B **721**, 94 (2013).

[53] W. Detmold, C.-J. D. Lin, and S. Meinel, Phys. Rev. D **85**, 114508 (2012).

[54] J. Flynn *et al.* (RBC and UKQCD Collaborations), *Proc. Sci.*, LATTICE2013 (2014) 408 [arXiv:1311.2251].

[55] F. Bernardoni, J. Bulava, M. Donnellan, and R. Sommer (ALPHA Collaboration), Phys. Lett. B **740**, 278 (2015).

[56] A. S. Kronfeld, Phys. Rev. D **62**, 014505 (2000).

[57] D. Arndt and C.-J. D. Lin, Phys. Rev. D **70**, 014503 (2004).

[58] A. Bazavov *et al.* (MILC Collaboration), *Proc. Sci.*, LATTICE2010 (2010) 074 [arXiv:1012.0868].

[59] S. Basak *et al.* (MILC Collaboration), *Proc. Sci.*, LATTICE2014 (2014) 116 [arXiv:1409.7139].

[60] E. Gregory, C. T. H. Davies, E. Follana, E. Gamiz, I. D. Kendall, G. P. Lepage, H. Na, J. Shigemitsu, and K. Y. Wong (HPQCD Collaboration), Phys. Rev. Lett. **104**, 022001 (2010).

[61] M. Atoui, V. Mornas, D. Beirevic, and F. Sanfilippo, Eur. Phys. J. C **74**, 2861 (2014).

[62] M. Guagnelli, F. Palombi, R. Petronzio, and N. Tantalo, Phys. Lett. B **546**, 237 (2002).

[63] M. Rotondo (private communication).

[64] D. Atwood and W. J. Marciano, Phys. Rev. D **41**, 1736 (1990).

[65] D. Buskulic *et al.* (ALEPH Collaboration), Phys. Lett. B **359**, 236 (1995).

[66] K. Abe *et al.* (Belle Collaboration), Phys. Lett. B **526**, 258 (2002).

[67] B. Aubert *et al.* (*BABAR* Collaboration), Phys. Rev. D **79**, 012002 (2009).

[68] J. E. Bartelt *et al.* (CLEO Collaboration), Phys. Rev. Lett. **82**, 3746 (1999).

[69] J. Lees *et al.* (*BABAR* Collaboration), Phys. Rev. Lett. **109**, 101802 (2012).

[70] A. Bazavov *et al.* (MILC Collaboration), Phys. Rev. D **87**, 054505 (2013).

[71] M. B. Oktay and A. S. Kronfeld, Phys. Rev. D **78**, 014504 (2008).

[72] J. A. Bailey *et al.* (Fermilab Lattice, MILC, and SWME Collaborations), *Proc. Sci.*, LATTICE2014 (2014) 097 [arXiv:1411.1823].

[73] J. A. Bailey, Y.-C. Jang, W. Lee, and J. Leem (SWME Collaboration), *Proc. Sci.*, LATTICE2014 (2014) 389 [arXiv:1411.4227].

[74] M. Nobes and H. Trottier, *Proc. Sci.*, LAT2005 (2006) 209 [arXiv:hep-lat/0509128].